

# Deuterium Enrichment of the Interstellar Medium

Ankan Das<sup>a</sup>, Liton Majumdar<sup>a</sup>, Sandip K. Chakrabarti<sup>b,a</sup>, Dipen Sahu<sup>a</sup>

<sup>a</sup>Indian Centre For Space Physics, 43 Chalantika, Garia Station Road, Kolkata 700084, India

<sup>b</sup>S.N. Bose National Center for Basic Sciences, JD-Block, Salt Lake, Kolkata, 700098, India

---

## Abstract

Despite low elemental abundance of atomic deuterium in interstellar medium (ISM), observational evidences suggest that several species in gas-phase and in ices could be heavily fractionated. We explore various aspects of deuterium enrichment by constructing a chemical evolution model in gas and grain phases. Depending on various physical parameters, gas and grains are allowed to interact with each other through exchange of their chemical species. It is known that  $\text{HCO}^+$  and  $\text{N}_2\text{H}^+$  are two abundant gas phase ions in ISM and their deuterium fractionation are generally used to predict degree of ionization in various regions of a molecular cloud. To have a more realistic estimation, we consider a density profile of a collapsing cloud. We present radial distributions of important interstellar molecules along with their deuterated isotopomers. We carry out quantum chemical simulation to study effects of isotopic substitution on spectral properties of these important interstellar species. We calculate vibrational (harmonic) frequency of the most important deuterated species (neutral & ions). Rotational and distortional constants of these molecules are also computed to predict rotational transitions of these species. We compare vibrational (harmonic) and rotational transitions as computed by us with existing observational, experimental and theoretical results. We hope that our results would assist observers in their quest of several hitherto unobserved deuterated species.

**Keywords:** Astrochemistry, spectra, ISM: molecules, ISM: abundances

---

## 1. Introduction

Study of deuterium enrichment received a major boost after discovery of singly or multiply deuterated  $\text{H}_2\text{CO}$  and  $\text{CH}_3\text{OH}$  in Interstellar Medium (ISM). Interestingly, fractionation ratios of these deuterated species often cross elemental D/H ratio of ISM ( $\sim 1.5 \times 10^{-5}$ , Linsky et al., 1995). Earlier work by Hasegawa, Herbst & Leung (1992); Chakrabarti et al. (2006ab); Das et al. (2008a); Das, Acharyya & Chakrabarti (2010); Cuppen & Herbst (2007); Das & Chakrabarti (2011) suggest that grain chemistry plays a crucial role in deciding chemical composition of ISM, in general. Role of grain

---

*Email addresses:* ankan@csp.res.in (Ankan Das), liton@csp.res.in (Liton Majumdar), chakraba@bose.res.in (Sandip K. Chakrabarti), dipen@csp.res.in (Dipen Sahu)

chemistry towards deuterium enrichment has been highlighted also by various authors (Caselli, 2002a; Cazaux et al., 2010; Das et al., 2013a). In gas phase, basic reactions are followed by dominant ion-molecular reaction pathways. Around the cold, dense region of the cloud, CO and O are heavily depleted from the gas phase. A strong correlation between the CO depletion and deuterium fractionation has been observed (Bacmann et al., 2003; Crapsi et al., 2005). Moreover, ionization of the ISM could be traced by observing some deuterated ions, such as,  $\text{DCO}^+$  and  $\text{N}_2\text{D}^+$  (Caselli, 2002a). So deuterium chemistry is extremely important for tracing dynamic properties of a cloud.

Aikawa et al. (2005), Das et al. (2008b), and Das et al. (2013b) already discussed how dynamic parameters of a cloud affect its chemical composition. Over the last two decades, several attempts were made to differentiate evolutionary stages of proto-stars. For example, Lada & Wilking (1984) defined three classes of proto-stars (Class I, Class II and Class III) which are progressively evolved. André et al. (1993) defined another class of proto-stars, namely, Class 0, which is the youngest among protostars. When Class 0 proto-stars are in a little more evolved stage, the source is considered to be a Class 0/I borderline object. These stages are defined by observing the variation of spectral energy distribution of protostars. A number of studies are carried out till date to find out a connection between abundances of chemical species and evolutionary stages (e.g., Smith, 1998; Myers et al., 1998; Forebrich, 2005) of a proto-star. A number of past studies suggest that the deuterium fractionation of some ions like  $\text{N}_2\text{H}^+$  and  $\text{HCO}^+$  could be used to define different evolutionary stages (Crapsi, 2005; Jørgensen et al., 2004). Recently, Majumdar et al. (2013) performed a quantum chemical calculation to obtain spectral signatures (infrared and electronic absorption spectra) of precursors of some bio-molecules such as adenine, alanine and glycine. It was found that spectral signatures of gas phase significantly differ from those in ice phase. Das et al. (2013a) discuss different properties of  $\text{HCOCN}$  and one of its isotopologues,  $\text{DCO}^+\text{CN}$ . This type of studies could also be carried out for other deuterated species which could serve as benchmarks for observation.

In this paper, we have presented a systematic approach to determine chemical evolution of some of the most important deuterated species and tried to present a complete spectral catalog for detecting these molecules around cold & dense regions of a molecular cloud. The plan of this paper is as follow: In Section 2, models and computational details are presented. Implications of our results are discussed in Section 3. Finally, in Section 4, we draw our conclusions.

## 2. Chemical Modeling

### 2.1. Gas phase Chemical Model

We prepare a large gas-grain chemical network to iteratively study chemical processes in a molecular cloud. Our gas phase chemical network consists of 6149 reactions among 601 species. We mainly follow the UMIST-2006 database (Woodall et al., 2007) for construction of our gas phase chemical network. Since in the present context, our motivation is to study deuterium enrichment of the ISM, we use some of the important reactions from UMIST-2006 database and assume that these reactions would also be possible for the deuterated isotopomers as well. Reaction rates are calculated by following the method used by Woodall et al. (2007). To avoid long computational time as

well as complexity in handling a large chemical network, we identify some dominant pathways for deuterium enrichment and concentrate on them. Our selection is based on earlier studies of Albertsson et al. (2013), Miller et al. (1989), Robert et al. (2000) and Rodgers & Millar (1996). We assume that gas and grains are coupled through accretion and thermal/cosmic ray evaporation processes. Details of these processes are already presented in Das & Chakrabarti (2011) and Das et al. (2013ab).

## 2.2. Ice phase Chemical Model

### 2.2.1. Accretion

Gas phase species are depleted by their accretion on interstellar ice. Following Hasegawa, Herbst & Leung (1992), accretion rate of a gas phase species is given by:

$$k_{acc}(i) = s_i \sigma v(i) n(i) s^{-1},$$

where,  $s_i$  is sticking coefficient,  $n(i)$  is gas phase concentration and  $v(i)$  is thermal velocity of  $i^{th}$  species,  $\sigma$  is geometrical dust-grain cross section ( $\sigma = 4\pi r^2$ ,  $r$  is the radius of the grain  $\sim 1000\text{\AA}$ ). In our simulation,  $s_i = 1$  is considered for all the neutrals except  $H_2$  and He. It is not certain wheather atomic and molecular ions stick to the grain surfaces (Hasegawa, Herbst & Leung, 1992; Watson, 1976), Here we considere  $s_i = 0$  for the ions.

### 2.2.2. Binding energies

Chemical enrichment of interstellar grain mantle solely depends on binding energies of surface species (Das & Chakrabarti, 2013). Mobility of lighter species such as H, D, N and O mainly dictates chemical composition of interstellar grain mantle. Composition of grain mantle which depends on mobility of H and O atoms are already discussed in Das et al. (2008a), Das, Acharyya & Chakrabarti (2010) and Das & Chakrabarti (2011). We assume that gas phase species are physisorbed onto dust grains ( $\sim 0.1\mu\text{m}$ ) having a grain number density of  $1.33 \times 10^{-12} n_H$ , where  $n_H$  is the concentration of H nuclei in all forms. Binding energies of deuterated species are assumed to be same as those of hydrogenated counterparts because binding energies of deuterated species are unknown. Several theoretical and experimental attempts were made till date to find out diffusion effects of atomic hydrogen. According to some past studies, as in Allen & Robinson (1977), Tielens & Allamandola (1987), Hasegawa & Herbst (1993), Hasegawa, Herbst & Leung (1992) and Chakrabarti et al. (2006ab), binding energy for diffusion ( $E_b$ ) of H atom was considered to be  $\sim 100$  K, whereas for desorption ( $E_d$ ), it was considered to be  $\sim 350$  K. Following Hasegawa & Herbst (1993), for  $H_2$  molecule, desorption energy was considered to be  $\sim 450$  K. According to Hasegawa & Herbst (1993) and references therein, adsorption energy of  $N_2$  is 1210 K. Caselli (2002a) and references therein, suggest that adsorption energy of  $N_2$  could be 787 K. In our simulation, we consider 787 K to be the adsorption energy for  $N_2$ . Desorption energies ( $E_d$ ) for all other species are taken from the past studies by Hasegawa & Herbst (1993). Following Tielens and Allamandola (1987) and Hasegawa, Herbst & Leung (1992), here also, we assume  $E_b=0.3E_d$  for all other species except for H atom. To show importance of these binding energies towards chemical complexity

of interstellar grain mantle, we construct three sets of binding energies. First Set consists of binding energies just mentioned above and we call it as set 1. Unless otherwise stated, we always use set 1 energy values. In set 2, we use results derived by Pirronello (1997, 1999) for binding energies ( $E_b$  and  $E_d$ ) of H and H<sub>2</sub> with olivine grain surface. So difference between set 1 and set 2 is that in set 2, we are using different binding energies ( $E_b$  and  $E_d$  both) for H, H<sub>2</sub>, D, HD and D<sub>2</sub> only. Binding energies of all other species are assumed to be similar to those belonging to the set 1. Similarly, in set 3, experimental findings of Pirronello (1997, 1999) for binding energies of H and H<sub>2</sub> with the amorphous carbon grain are used. For more clarity, in Table 1, we give these three sets of binding energies. Since for all cases binding energies of all the species except H, D, H<sub>2</sub>, HD, and D<sub>2</sub> are similar, we only tabulate the binding energies ( $E_b$  and  $E_d$ ) of these species only. For the sake of completeness in Table 1, we have shown the binding energies of some important surface species (O, OH, H<sub>2</sub>O, CO, H<sub>2</sub>CO, CH<sub>3</sub>OH) as well.

### 2.2.3. Reaction

There are two reaction schemes, the Langmuir-Hinshelwood (LH) mechanism and the Eley-Rideal (ER) mechanism normally considered for the surface reactions. In the LH scheme, the gas phase species accretes onto a grain and becomes equilibrated with the surface before it reacts with another atom or molecule, and in the ER reaction scheme, the incident gas phase species collides directly with an adsorbed species on the surface and reacts with that species. In order to react, the adsorbed species require sufficient mobility. Surface reaction rate  $R_{i,j}$  between surface species  $i$  and  $j$  occurring due to classical diffusion can be expressed as (Hasegawa et al., 1992),

$$R_{i,j} = k_{i,j}(Rdiff_i + Rdiff_j)n_i n_j n_d,$$

where,  $n_i$  and  $n_j$  are the number of species  $i$  and  $j$  respectively, on an average grain,  $Rdiff_i$  and  $Rdiff_j$  are the diffusion rate (defined as inverse of the diffusion time),  $k_{i,j}$  is the probability for the reaction to happen upon an encounter. The parameter  $k_{i,j}$  is in general unity for the exothermic reaction without activation energy. For an exothermic reaction with activation energy  $E_a$  and at least one light reactant (H, H<sub>2</sub>),  $k_{i,j}$  can be approximated by the exponential portion of the quantum mechanical probability for tunneling through a rectangular barrier of thickness  $a$ :

$$k_{i,j} = \exp[(-4\pi a/h)(2\mu E_a)^{1/2}],$$

where,  $\mu$  is the reduced mass and  $a$  is taken as 1 Å. For the light reactive species H and H<sub>2</sub>, surface migration via tunneling is much faster than that due to classical hopping. The time scale for tunneling is given by,

$$t_{tun} = \nu_0^{-1} \exp[(4\pi a/h)(2mE_b)^{1/2}] \text{ sec.}$$

For the grain surface reaction network, we primarily follow Hasegawa, Herbst & Leung (1992), Cuppen & Herbst (2007), Das, Acharyya & Chakrabarti (2010) and Das & Chakrabarti (2011). For deuterium fractionation reaction on the grain surface, we primarily follow Caselli (2002a) and Cazaux et al. (2010).

Table 1: Various sets of binding energies

Species	set 1		set 2		set 3	
	$E_b$	$E_d$	$E_b$	$E_d$	$E_b$	$E_d$
H	100	350	287	373	511	657
H <sub>2</sub>	135	450	95	315	163	542
D	100	350	287	373	511	657
HD	135	450	95	315	163	542
D <sub>2</sub>	135	450	95	315	163	542
O	240	800	240	800	240	800
OH	378	1260	378	1260	378	1260
H <sub>2</sub> O	558	1860	558	1860	558	1860
CO	363	1210	363	1210	363	1210
H <sub>2</sub> CO	528	1760	528	1760	528	1760
CH <sub>3</sub> OH	618	2060	618	2060	618	2060

Table 2: Initial abundances

Species	Abundance
H <sub>2</sub>	$5.00 \times 10^{-01} / n_H$
He	$1.00 \times 10^{-01} / n_H$
N	$2.14 \times 10^{-05} / n_H$
O	$1.76 \times 10^{-04} / n_H$
H <sub>3</sub> <sup>+</sup>	$1.00 \times 10^{-11} / n_H$
C <sup>+</sup>	$7.30 \times 10^{-05} / n_H$
S <sup>+</sup>	$8.00 \times 10^{-08} / n_H$
Si <sup>+</sup>	$8.00 \times 10^{-09} / n_H$
Fe <sup>+</sup>	$3.00 \times 10^{-09} / n_H$
Na <sup>+</sup>	$2.00 \times 10^{-09} / n_H$
Mg <sup>+</sup>	$7.00 \times 10^{-09} / n_H$
P <sup>+</sup>	$3.00 \times 10^{-09} / n_H$
Cl <sup>+</sup>	$4.00 \times 10^{-09} / n_H$
e <sup>-</sup>	$7.31 \times 10^{-05} / n_H$
HD	$1.60 \times 10^{-05} / n_H$
H	$1.00 \times 10^{00} \text{ cm}^{-3}$
D	$1.00 \times 10^{-01} \text{ cm}^{-3}$

#### 2.2.4. Thermal evaporation

In our model, abundances of surface species could be decreased by thermal evaporation, cosmic ray induced evaporation and non-thermal desorption processes. Rate of thermal evaporation of the surface species ‘i’ could be calculated by the following relation,

$$k_{evap}(i) = \nu_0 \exp(-E_d/kT_g) \text{ sec}^{-1}, \quad (1)$$

where,  $\nu_0$  is characteristic vibrational frequency ( $\nu_0 = \sqrt{2n_s E_d / \pi^2 m}$ ) and  $T_g$  is temperature of grain. For all cases, we have considered that total number of sites ( $N_s$ ) on a grain is  $10^6$  having surface density of sites ( $n_s$ ) of  $2 \times 10^{14} \text{ cm}^{-2}$ .

### 2.2.5. Cosmic ray induced evaporation

Cosmic ray induced evaporation (hereafter CRD) is a very efficient means to transfer surface molecules into gas phase during late stage of chemical evolution. Cosmic ray induced evaporation rates are calculated by using the expression developed by Hasegawa & Herbst (1993). Following Leger et al. (1985), they assumed that relativistic Fe nuclei with energies 20 – 70 MeV could deposit 0.4 MeV energy on an average dust particle of radius  $0.1 \mu\text{m}$ . Grains could be cooled down due to thermal evaporation and radiation processes. For easy inclusion of cosmic ray induced photo-evaporation into their model, they developed the following relation:

$$k_{\text{crd}} \sim f(70, K)k_{\text{evap}}(i, 70 \text{ K}), \quad (2)$$

where,  $k_{\text{evap}}(i, 70 \text{ K})$  is the thermal evaporation rate of surface species ‘i’ at temperature 70 K,  $f(70 \text{ K})$  is fraction of time spent by grains at around 70 K. Following Leger et al. (1985), they defined  $f(70 \text{ K}) = 3.16 \times 10^{-19}$ .

### 2.2.6. Non thermal desorption

Because energy is released during some of the reactions, adsorbed species could desorb just after their formation. Garrod et al. (2007) estimated desorption rate via exothermic surface reactions by considering Rice-Ramsperger-Kessel (RRK) theory. They parameterized non-thermal desorption by assuming some approximation. They assumed that a fraction ‘f’ of the product species in qualifying reactions could desorb immediately and the rest (1-f) fraction remains as a surface bound product. Here, we apply this mechanism to all surface reactions which result in a single product. Fraction ‘f’ is calculated by;

$$f = \frac{aP}{(1 + aP)}, \quad (3)$$

where,  $a$  is ratio between surface molecule bond frequency to frequency at which energy is lost to grain surface. Garrod et al. (2007), adopted similar  $a$  values for all the species. They varied  $a$  from 0.01 to 0.1. A value of  $a = 0.1$  was labeled as ‘high’ by Pilling (2006). Kroes & Andersson (2006) carried out molecular dynamics simulations of the irradiation of water ice with UV photons. From their data, Garrod et al. (2007) estimated that  $\sim 0.9\%$  of recombinations result in desorption. Using the value of  $E_D(\text{H}_2\text{O}) = 5700 \text{ K}$  and  $E_{\text{reac}} = 5.91 \times 10^4 \text{ K}$ , they had  $a = 0.012$ . Recently, Dulieu et al. (2013) experimentally found that 90 % of  $\text{H}_2\text{O}$  formed on surfaces with  $\text{OH} + \text{H}$  is directly released into the gas phase (Dulieu et al. 2013). But this is yet to be verified for the other species. Here we are considering a huge gas-grain chemical network. In order to test the effects of the non-thermal desorption mechanism and constrain the value of  $a$ , we investigate models with various values of  $a$  : 0, 0.01, 0.05, 0.1. To be on the safer side, we choose an intermediate value of  $a$  ( $a = 0.05$ ) for all surface reactions.

## 2.3. Results of chemical modeling

Hydrogen molecules are mainly formed in diffuse regions evolving into molecular clouds through surface chemistry. In this study, we aim at studying chemical evolution of a molecular cloud into dense cores. For this purpose, we adopt initial conditions

Table 3: Fractionation ratios of the Ice phase species for various sets of energies

Species	Isotopomers	Fractionation ratio (column density in $\text{cm}^{-2}$ ) by using set 1	Fractionation ratio (column density in $\text{cm}^{-2}$ ) by using set 2	Fractionation Ratio (column density in $\text{cm}^{-2}$ ) by using set 3	Fractionation ratio (column density in $\text{cm}^{-2}$ ) by using experimental activation barrier along with set 1
$\text{H}_2\text{O}$	HDO	$9.93 \times 10^{-02} (1.62 \times 10^{17})$	$1.97 \times 10^{-01} (2.47 \times 10^{17})$	$2.11 \times 10^{-02} (4.60 \times 10^{16})$	$6.99 \times 10^{-02} (1.40 \times 10^{17})$
	$\text{D}_2\text{O}$	$1.39 \times 10^{-03} (2.26 \times 10^{15})$	$1.10 \times 10^{-04} (1.38 \times 10^{14})$	$9.42 \times 10^{-05} (2.05 \times 10^{14})$	$5.72 \times 10^{-04} (1.15 \times 10^{15})$
$\text{H}_2\text{CO}$	HDCO	$5.37 \times 10^{00} (2.89 \times 10^{10})$	$2.08 \times 10^{-01} (1.35 \times 10^{15})$	$5.35 \times 10^{-02} (2.61 \times 10^{16})$	$4.84 \times 10^{02} (9.53 \times 10^{07})$
	$\text{D}_2\text{CO}$	$8.24 \times 10^{-02} (4.43 \times 10^{08})$	$7.46 \times 10^{-04} (4.84 \times 10^{12})$	$5.40 \times 10^{-04} (2.63 \times 10^{14})$	$1.10 \times 10^{02} (2.16 \times 10^{05})$
$\text{CH}_3\text{OH}$	$\text{CH}_3\text{OD}$	$3.06 \times 10^{-02} (1.11 \times 10^{16})$	$4.19 \times 10^{-03} (1.24 \times 10^{15})$	$9.39 \times 10^{-03} (5.22 \times 10^{11})$	$1.01 \times 10^{-02} (6.06 \times 10^{15})$
	$\text{CH}_2\text{DOH}$	$8.24 \times 10^{-02} (2.98 \times 10^{16})$	$8.84 \times 10^{-02} (2.62 \times 10^{16})$	$6.12 \times 10^{-02} (3.40 \times 10^{12})$	$1.14 \times 10^{-02} (6.85 \times 10^{15})$
	$\text{CHD}_2\text{OH}$	$1.09 \times 10^{-03} (3.94 \times 10^{14})$	$2.55 \times 10^{-04} (7.55 \times 10^{13})$	$7.11 \times 10^{-04} (3.95 \times 10^{10})$	$4.59 \times 10^{-02} (2.75 \times 10^{16})$
	$\text{CD}_3\text{OH}$	$1.06 \times 10^{-07} (3.82 \times 10^{10})$	$4.59 \times 10^{-09} (1.36 \times 10^{09})$	$3.97 \times 10^{-07} (2.20 \times 10^{07})$	$2.43 \times 10^{-04} (1.45 \times 10^{14})$
	$\text{CD}_3\text{OD}$	$3.11 \times 10^{-09} (1.13 \times 10^{09})$	$2.10 \times 10^{-11} (6.24 \times 10^{06})$	$2.88 \times 10^{-10} (1.60 \times 10^{04})$	$2.98 \times 10^{-06} (1.78 \times 10^{12})$
	$\text{CH}_2\text{DOD}$	$2.14 \times 10^{-03} (7.73 \times 10^{14})$	$3.69 \times 10^{-04} (1.10 \times 10^{14})$	$9.52 \times 10^{-02} (1.10 \times 10^{16})$	$2.51 \times 10^{-04} (1.50 \times 10^{14})$
	$\text{CHD}_2\text{OD}$	$2.71 \times 10^{-05} (9.80 \times 10^{12})$	$1.16 \times 10^{-06} (3.44 \times 10^{11})$	$6.60 \times 10^{-06} (3.67 \times 10^{08})$	$4.97 \times 10^{-04} (2.98 \times 10^{14})$
	$\text{CH}_3\text{OD}$				

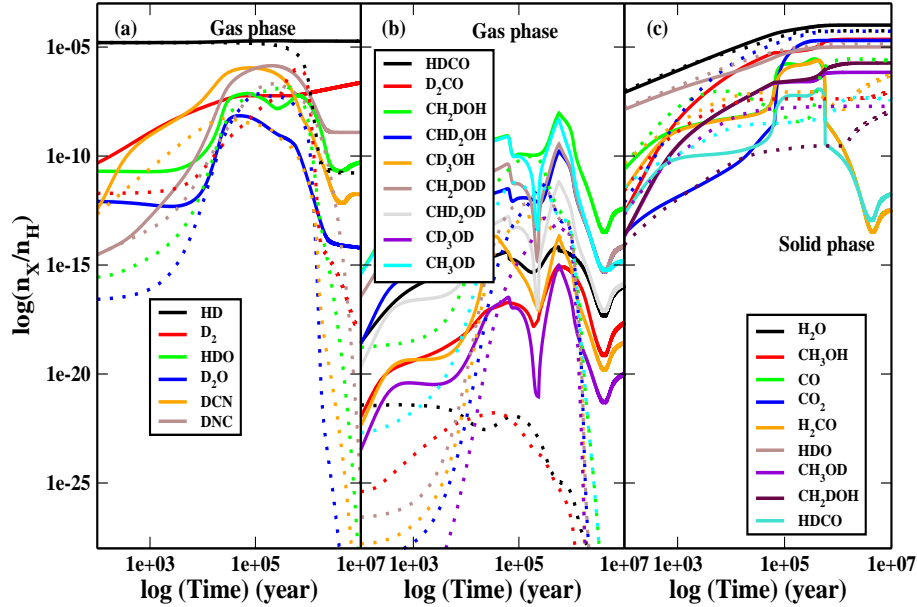


Figure 1: Chemical evolution of some important gas(a,b) and ice(c) phase neutral deuterated species in ISM. Solid lines are for cases where CRD and non-thermal desorption effects are considered and dotted lines are for cases where these two effects are not considered.

from molecular clouds, where almost all hydrogens are in the form of molecular hydrogen, and temperature of gas and dust are assumed to be  $\sim 10$  K. Ionization in these regions is mainly governed by Cosmic rays. We adopt an initial condition by following Leung, Herbst & Huebner (1984) (Table 2). They considered two sets of initial conditions (i) when metallicity is high and (ii) when metallicity is low. For set (ii) S, Si, Na, Mg and Fe are assumed to be depleted by two orders of magnitude as compared to set (i). Leung, Herbst & Huebner (1984) found that results of set (i) agree better with observed molecular abundances in cool, dense clouds. Here also we are considering a similar initially low metallicity condition. It is assumed that initially all deuteriums could be locked in the form of HD (just as we assumed that all H are in the form of hydrogen molecules initially). Initial abundance of HD molecule is assumed to be  $1.6 \times 10^{-5}$  with respect to total hydrogen nuclei. Initial abundance of atomic form of hydrogen and deuterium are considered to be  $1 \text{ cm}^{-3}$  and  $0.1 \text{ cm}^{-3}$  respectively. Unless otherwise stated, we always use initial abundance given in Table 2.

### 2.3.1. Neutral deuterated species

In Fig. 1ab, chemical evolution of some important gas phase neutral deuterated species with respect to total hydrogen ( $n = n_H + 2 \times n_{H_2}$ ) are shown. Here, we assume that the cloud is at  $T = 10$  K having constant number density ( $n = 10^4 \text{ cm}^{-3}$ ), visual extinction  $A_V = 10$ . Solid lines of Fig. 1ab, represent chemical evolution of gas phase species, where we have considered CRD and non-thermal desorption effects. Dotted lines are for the cases where we have not considered CRD and non-thermal desorption effects. As expected, CRD and non-thermal desorption serve as efficient means to maintain a reasonable gas phase abundance during later stages of chemical evolution process. Due to depletion of gas phase deuterated species, curves show a decreasing trend after achieving a peak value. Solid lines show that gas phase species are maintained in a steady state equilibrium because of the effects of CRD and non-thermal desorption. Figure 1a clearly shows that HD molecule is the most abundant deuterated gas phase species throughout the evolution.  $D_2$  is also found to be significantly abundant. Initially, all deuteriums were locked in the form of HD molecule. By virtue of low binding energies with grain surface, HD and  $D_2$  maintain high abundances during late stages of chemical evolution process. Two isotopomers of  $H_2O$  (HDO and  $D_2O$ ) and HCN (DCN and DNC) are found to be significantly abundant in gas phase. Chemical evolution of several isotopomers of  $CH_3OH$  and  $H_2CO$  are shown in Fig. 1b. Singly deuterated isotopomers of methanol ( $CH_3OD$ ,  $CH_2DOH$ ) are found to be reasonably abundant. Along with doubly and triply deuterated isotopomers, tetra deuterated isotopomer is found to be produced in gas phase as well. Abundance of HDCO and  $D_2CO$  are also significant while we are considering CRD and non-thermal desorption effects. These molecules are most likely formed on dust surfaces during cold, dense pre-collapse period and are evaporated to the gas phase (Loinard et al., 2000). From Fig. 1ab, it is clear that when CRD and non-thermal desorption effects are taken into account, abundances of gas phase species reach a steady state equilibrium beyond  $10^6$  year. Species attain their peak values  $\sim 1 \times 10^5$  year. Depending on physical condition (density and temperature), accretion rate of the gas phase species changes. As per Caselli (2002a), for a normal dust to gas ratio and assuming typical dust grains with radius of  $0.1 \mu\text{m}$ , the *average* time scale for a gaseous species to be deposited onto a



grain is

$$t_D \sim 10^9 \sqrt{(A_X)/[S n(H_2)]} \text{ year},$$

where,  $A_X$  is molecular weight,  $S$  is sticking coefficient and  $n(H_2)$  is number density of molecular hydrogen. Sticking coefficient of all neutral species are assumed to be unity. Results presented in Fig. 1ab are for the number density ( $n_H$ ) =  $10^4 \text{ cm}^{-3}$  (i.e., for  $n_{H_2} = 5 \times 10^3 \text{ cm}^{-3}$ ). From the above equation the time scale for depleting species from the gas is  $\sim 1 \times 10^5$  years. As depletion is inversely proportional to the density, for high density cloud, depletion time would be much shorter.

In Fig. 1c, chemical evolution of the most abundant surface species ( $H_2O$ ,  $CO$ ,  $CO_2$ ,  $H_2CO$ ,  $CH_3OH$ ) along with their most abundant deuterated analogues ( $HDO$ ,  $HDCO$ ,  $CH_3OD$ ,  $CH_2DOH$ ) are shown. As gas phase species deplete in around  $2 \times 10^5$  years, we are obtaining a steady state for the abundances of surface species beyond that time. Singly deuterated water, formaldehyde and methanol are found to be heavily abundant. From Fig. 1b, significant difference between gas phase abundances of these species for two cases (with CRD and non-thermal desorption process and without these effects) are distinctly visible. Gas-phase abundances of species like methanol and formaldehyde cannot be explained by gas-phase chemistry alone. In fact, the sole potential synthesis of these species seems to be production on surfaces of interstellar grains followed by desorption into the gas. Yet, thermal evaporation process (binding energies of these species with grain surfaces are much higher  $\sim 2000 \text{ K}$ ) is inefficient for explaining abundances of molecules such as methanol and formaldehyde at around  $10 \text{ K}$ . It is necessary then to contemplate non-thermal mechanisms as natural processes. Formaldehyde and methanol are mainly formed by hydrogenation reaction of  $CO$  on interstellar dust grains, and are released in the gas phase in hot core regions. Noble et al. (2012) recently performed experiments to study various desorption processes. Another interesting point to be noted from Fig. 1c is that surface abundances of  $CH_3OH$  and its deuterated isotopomers increase when we consider non-thermal desorption process (solid lines). It was expected that inclusion of non-thermal desorption parameter will increase gas phase abundances of these species by virtue of decrease of surface abundances of these species. But as in Garrod et al. (2007), here also we notice a strong enhancement of surface abundances of methanol along with its deuterated isotopomers. Garrod et al. (2007) mentioned that when non-thermal desorption effect were not considered, most of the surface methanol channeled into  $CH_4$  at late times. But when non-thermal desorption process was considered, carbon hydrides are allowed to return to gas phase, where they could convert into  $CO$  or its hydrides and maintain a modest level of  $CO$ , formaldehyde and methanol in both gas phase and on grain surfaces. In order to study effects of non-thermal desorption on these species, we assumed various ‘ $a$ ’ values and have separately presented results in Fig. 2. Three curves are shown for formaldehyde and methanol with  $a = 0$ ,  $a = 0.01$  and  $a = 0.1$ . As expected, for higher ‘ $a$ ’ values, gas phase abundances of formaldehyde and methanol are enhanced. During late stages of chemical evolution, gas phase abundance of these species are significant due to non-thermal desorption process. So it is essential to consider non-thermal desorption process into any gas-grain chemical model especially for low temperature regime. From now on, we consider the intermediate value of ‘ $a$ ’, namely,  $a = 0.05$ .

Chemical composition resulting from our model solely depends on initial abun-

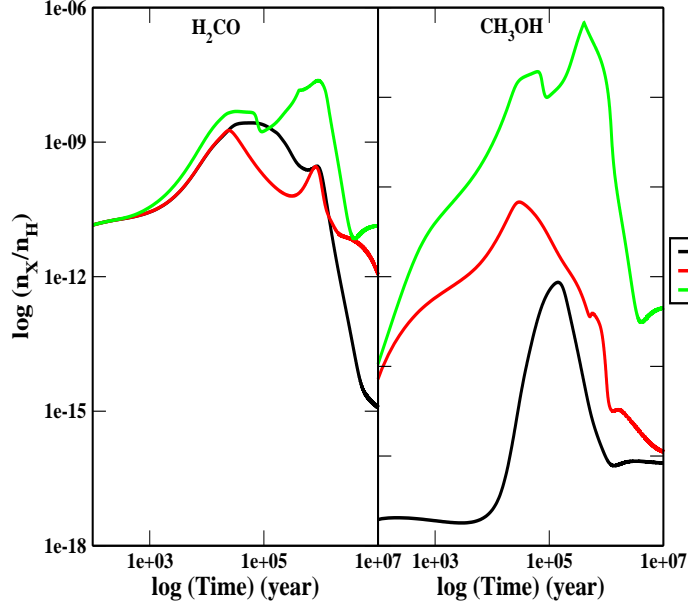


Figure 2: Chemical evolution of gas phase  $\text{H}_2\text{CO}$  and  $\text{CH}_3\text{OH}$  are shown for various values of ‘ $a$ ’.

dances considered. In order to test this feature, we consider a similar physical condition for carbon rich environment. Unless otherwise stated, we always consider initial abundances of  $\text{C}^+$  to be  $7.3 \times 10^{-5}$ . To mimic a carbon rich environment, we assume high carbon abundance initially ( $1.4 \times 10^{-4}$  relative to hydrogen nuclei) in ionized ( $\text{C}^+$ ) and in the neutral (C) form. For the purpose of illustration, chemical evolution of  $\text{HCO}^+$  is shown in Fig. 3. Abundance of  $\text{HCO}^+$  vary significantly with the choice of initial form (ionized or neutral) and abundance of carbon. For higher initial  $\text{C}^+$  abundance, we have much higher  $\text{HCO}^+$  as expected and for higher neutral carbon abundance, we have much lower  $\text{HCO}^+$  abundance as expected.

### 2.3.2. Deuterated ions

In Fig. 4, we show chemical evolution of the most important deuterated molecular ions;  $\text{DCO}^+$ ,  $\text{N}_2\text{D}^+$ ,  $\text{H}_2\text{D}^+$ ,  $\text{HD}_2^+$ ,  $\text{H}_2\text{DO}^+$ ,  $\text{HD}_2\text{O}^+$ ,  $\text{D}_3\text{O}^+$ ,  $\text{HDCN}^+$ ,  $\text{D}_2\text{CN}^+$ ,  $\text{DCN}^+$ ,  $\text{C}_3\text{D}^+$  and  $\text{CD}^+$ . Figure 4 clearly shows that beyond  $2 \times 10^5$  years, abundances of these gas phase deuterated ions decrease gradually. Due to depletion of neutrals in around  $2 \times 10^5$  years, production of related ions are also heavily hindered. Since recombination rate coefficients (reaction with electrons) of these ions are much higher ( $\sim 10^{-6}$  to  $10^{-7} \text{ cm}^3\text{s}^{-1}$ ), destruction rate of ions is much faster than the production rate. As a result, ions are disappearing at the same time scale as the neutrals. Among these ions,  $\text{DCO}^+$  and  $\text{N}_2\text{D}^+$  are widely used to correlate degree of ionization of ISM. Figure 4

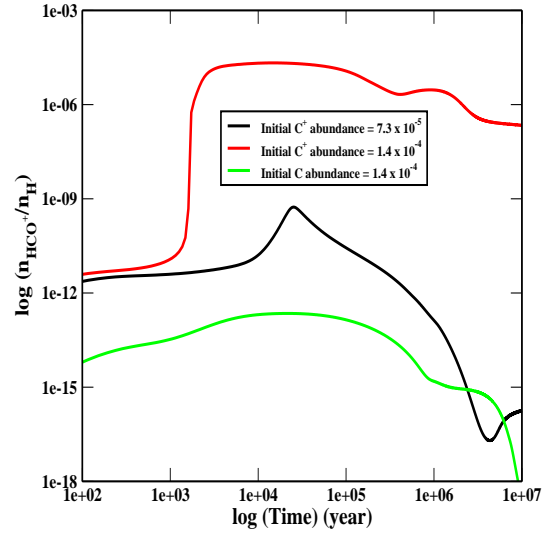


Figure 3: Chemical evolution of gas phase  $\text{HCO}^+$  for various initial carbon abundances.

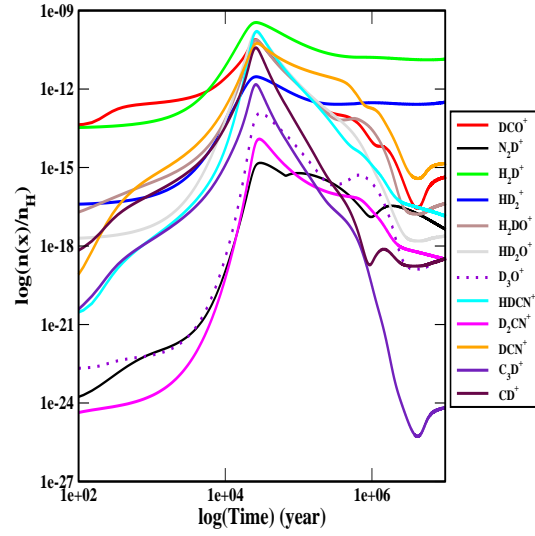
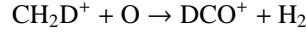
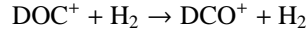
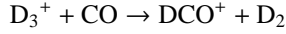
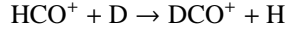
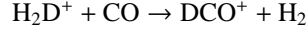
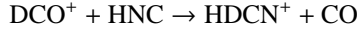
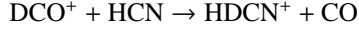
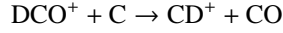
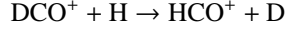
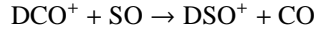
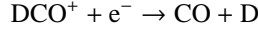


Figure 4: Important deuterated molecular ions in gas phase.

shows that DCO<sup>+</sup> molecule is very abundant in the gas phase. The ratio DCO<sup>+</sup>/HCO<sup>+</sup> (hereafter  $R_1$ ) is widely used as a measure of limit on electron abundances ( $x_e$ ) in ISM. According to Roberts & Millar (2000), at low temperatures, DCO<sup>+</sup> is primarily formed via  $H_2D^+ + CO \rightarrow DCO^+ + H_2$ . But there are other efficient routes for the formation of this species. Here, we have followed pathways mentioned in Albertson et al. (2013) and Robert & Millar (2000) for production and destruction of DCO<sup>+</sup>. According to Albertsson et al. (2013), major formation routes of DCO<sup>+</sup> are the followings;



and major destruction routes are the followings,



### 2.3.3. Modeling for a Molecular cloud

To have results under a more realistic situation, and to have radial distribution of various interstellar species, we now consider that density profile follows  $\rho \sim r^{-2}$  distribution as described by Shu (1977). Here we consider that inner boundary of protostar is at 100AU and outer boundary was chosen in such a way that density would become  $10^4 \text{ cm}^{-3}$ . In Fig. 5, density profile of the collapsing cloud is shown. In our simulations, we evolve our chemical code for various values of number densities of total hydrogen nuclei ( $n_H$ ) up to life time of a generic molecular cloud ( $\sim 10^7$  years). For the sake of simplicity, we assume that from the beginning, ( $t = 0$ ) this cloud maintains this density profile. Initial conditions are assumed to be similar to the initial conditions of a molecular cloud. We picked up different density at various regions of the cloud (from Fig. 5) and studied chemical evolution of these regions. For all cases, it was assumed that  $T = 10$  K and  $A_V = 10$ .

In order to test depletion time scale of CO and N<sub>2</sub>, in Fig. 6, we show chemical evolution of CO and N<sub>2</sub> at two different density regions of the cloud. Solid lines are for  $n_H = 10^4 \text{ cm}^{-3}$  and dotted lines are for  $n_H = 10^7 \text{ cm}^{-3}$ . For both cases, CO is depleted much earlier than N<sub>2</sub>. In case of  $n_H = 10^4 \text{ cm}^{-3}$ , around  $\sim 2 \times 10^6$  year CO molecules are heavily depleted whereas for  $n_H = 10^7 \text{ cm}^{-3}$ , this depletion time scale

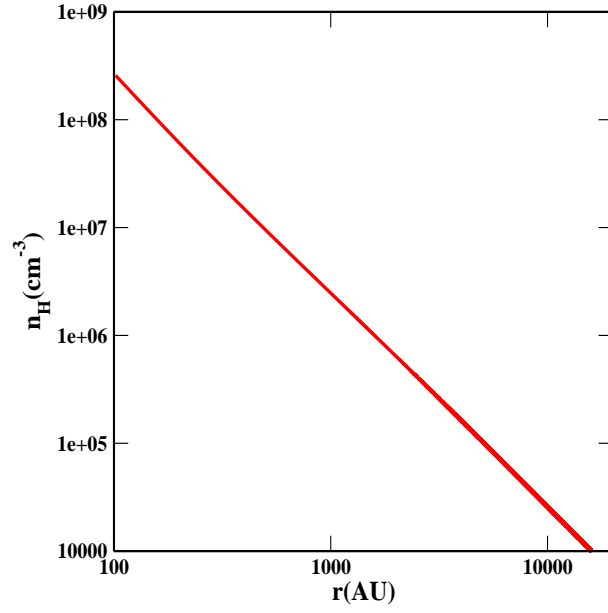


Figure 5: Density profile of a collapsing cloud.

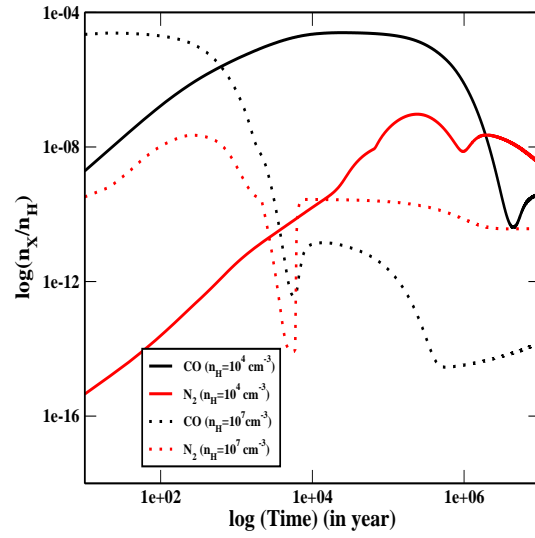


Figure 6: Chemical evolution of gas phase CO and N<sub>2</sub> for  $n_H = 10^4 \text{ cm}^{-3}$  and  $n_H = 10^6 \text{ cm}^{-3}$ .

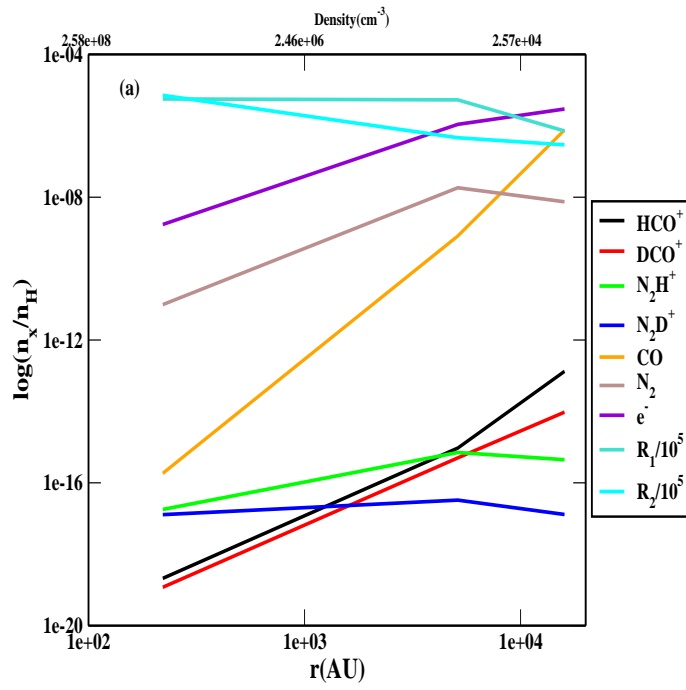


Figure 7: Radial distribution of some important gas phase ions,  $R_1$ ,  $R_2$  along with  $\text{CO}$ ,  $\text{N}_2$  and  $e^-$ .

is shifted by about  $\sim 8 \times 10^3$  year. In case of  $N_2$ , depletion features were obtained but it maintains higher abundances during the later stages. This is mainly because of low binding energy of  $N_2$  ( $E_d = 787$  K) in comparison to that of CO ( $E_d = 1210$  K) with grain surfaces. Deuterated species are normally used to trace slightly warmer region of the core.  $R_1$  is normally used to co-relate ionization degree ( $n_e/n_H$ ) of ISM. But species like CO could be depleted at their dense interior (clearly visible from Fig. 6) and could severely affect  $R_1$ . In order to justify appropriate deuterium fractionation of an entire core, one has to observe molecules that are less affected by depletion, such as  $N_2H^+$  and  $NH_3$ . Another benefit of observing N-bearing molecules is that their emission lines are splitted into hyperfine components due to non-zero nuclear spin of nitrogen, enabling optical depths of intervening medium to be measured. So it is customary to study the ratio  $N_2D^+/N_2H^+$  (hereafter  $R_2$ ) to have a better approximation around that region.

Figure 7 shows abundances of  $HCO^+$ ,  $DCO^+$ ,  $N_2H^+$  and  $N_2D^+$  at various depths. Abundances are taken from our simulation results at  $t = 10^6$  year. From Fig. 7, it is clear that as density increases inside, abundances of all gas phase ions decreases. In Fig. 6, we have shown that  $N_2$  molecules deplete more slowly due to lower binding energies. A similar thing is also seen in Fig. 7. Figure 7 shows that deep inside the cloud CO depletes heavily.  $N_2$  is also depleted but its rate of depletion is much slower in comparison to CO. As a result, CO related species ( $HCO^+$  and  $DCO^+$ ) are depleting heavily, whereas  $N_2$  related species ( $N_2D^+$  and  $N_2H^+$ ) depletes very slowly around the dense interior. Radial distributions of  $R_1$  and  $R_2$  along with the abundance of  $e^-$  are also shown in Fig. 7. From Fig. 7, it is noted that  $R_1$  remains roughly constant deep inside, while  $R_2$  steadily increases with depth. This implies that as we go inside the cloud and density increases, deuterium fractionation of  $N_2H^+$  becomes favourable. However, in case of  $HCO^+$ , deuterium fractionation roughly remains constant.

In Fig. 8, we plot electron abundance (a) with respect to  $R_1$  and (b) with respect to  $R_2$ . It is already mentioned that due to heavy depletion of CO and its related species around the dense interior,  $N_2$  related species should be used to predict the degree of ionization ( $n_e/n_H$ ). We divide the entire zone of molecular clouds in two parts: first one is the outer shell (extended from 6000AU to 20000AU) and second one is the dense interior (extended from 100AU to 6000 AU).  $R_1$  could be used to trace degree of ionization of the outer shell. From our model, we have electron abundance in the range of  $10^{-6} - 3 \times 10^{-6}$ . From Fig. 8a, we have the following relation between electron abundance and  $R_1$  in between 100AU to 6000 AU.

$$\frac{n_e}{n_H} = 3.2502 \times 10^{-6} - 4.0302 \times 10^{-6} R_1.$$

In the dense interior (100AU - 6000AU),  $R_2$  should be used to measure the degree of ionization. From our model, this is in the range of  $10^{-9} - 10^{-6}$  in this region. It has the following relation (Fig. 8b):

$$\frac{n_e}{n_H} = 6.3773 \times 10^{-6} - 0.00012136 R_2 + 0.00015693 R_2^2$$

In reality, ionization degree depends on various parameters.  $R_1$  and  $R_2$  could be used to diagonalize it to some extent. Since, abundance of any species depends on various

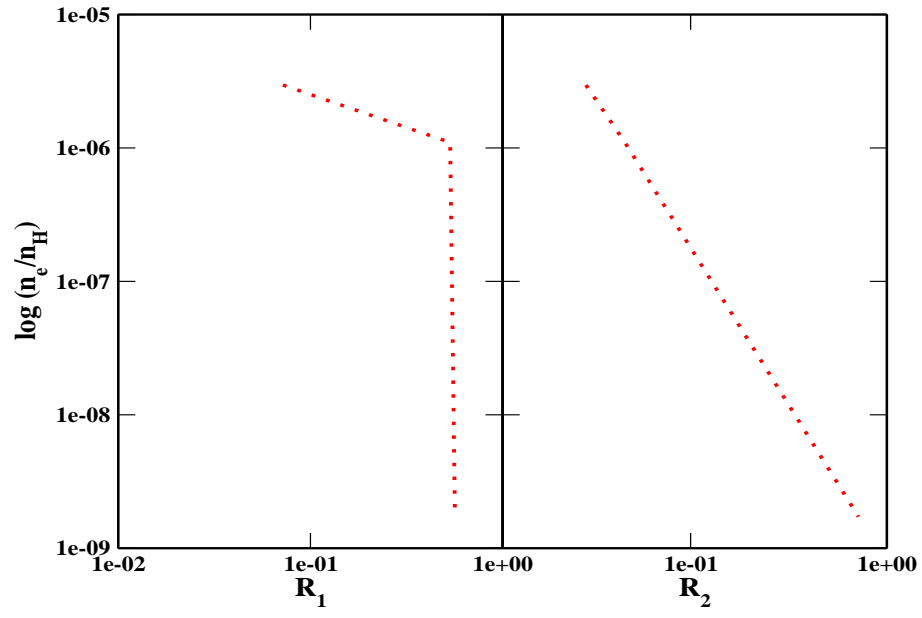


Figure 8: Electron abundance relative to (a)  $R_1$  and (b)  $R_2$ .



physical conditions and age of the source, it is very difficult to present any generalized formula for predicting the ionization degree at any particular instant.

So far, a number of theoretical models tried to correlate physical properties of protostars with time since gravitational collapse begins (e.g., Smith, 1998; Myers et al., 1998). Time sequences of evolutionary stages determined by various models are more or less similar but absolute ages vary significantly (Emprechtinger et al., 2008 and references therein). According to Froebrich (2005), absolute age for Class 0/I borderline objects, for example, varies between  $10^4$  years and a few times  $10^5$  years. According to Emprechtinger et al. (2008),  $R_2$  is known to trace the evolution of prestellar cores. They proposed that  $R_2$  could be used to trace core evolution even after the star formation. According to them, protostars with  $R_2 > 0.5$  are in a stage shortly after beginning of collapse. Later on,  $R_2$  decreases until it reaches a value of 0.03 at Class 0/I borderline.

Several deuterated molecules are found to be heavily abundant in ISM. Even water could also be highly fractionated. HDO could efficiently be formed on the grain surfaces by the deuteration reaction. Stark et al. (2004) reported detection of HDO ground transition towards IRAS 16293 and derived a HDO abundance of  $\sim 10^{-10}$  in cold region of the envelope. Measurement of water deuterium fractionation is a relevant tool for understanding mechanisms of water formation and evolution from prestellar phase to formation of planets and comets (Coutens et al., 2013). Several attempts were made to derive HDO/H<sub>2</sub>O ratio for various Class 0 protostars, which correspond to main accretion phase. But results turned out to be quite different from one another. Measurements of HDO/H<sub>2</sub>O were carried out at two separate zones. For  $T > 100$  K, region of IRAS 16293-2422, Parise et al. (2005) and Coutens et al. (2012, 2013) estimated a HDO/H<sub>2</sub>O ratio about a few percent, using single dish observations, whereas Persson et al. (2013) found much lower estimate ( $9 \times 10^{-4}$ ) using interferometric data. For  $T < 100$  K region, the ratio of HDO/H<sub>2</sub>O found to be between  $3 \times 10^{-3} - 1.5 \times 10^{-2}$  in IRAS 16293-2422 by Coutens et al. (2012, 2013).

A large amount of doubly deuterated formaldehyde (D<sub>2</sub>CO) has been observed in solar type proto-star IRAS 16293-2422 (Ceccarelli et al., 1998). Turner (1990) found that D<sub>2</sub>CO/H<sub>2</sub>CO  $\sim 0.003$  in the Orion compact ridge. It was expected that this high fractionation of D<sub>2</sub>CO occurs on the grain during the cold phase and that the species are evaporated to gas component during warm phase. Moreover, a detection of doubly deuterated and triply deuterated methanol was reported by Parise et al. (2002, 2004) towards low mass protostar IRAS 16293-2422.

In Fig. 9abc, we show deuterium fractionation ratio of some of the major ice phase species with variation of initial atomic D/H ratio of gas phase. In the study from Roberts et al. (2003) the D/H ratio can reach 0.3. Here, we vary the initial atomic D/H ratio from  $10^{-5}$  to 1. For this case, we consider set 1 energy values,  $n_H = 10^4$  cm<sup>-3</sup>,  $T=10$ K,  $A_V = 10$  and vary initial atomic D/H ratio. Deuterium fractionation values are taken during the late time (beyond  $\sim 10^6$  year). Figure 9abc clearly shows that singly deuterated part of H<sub>2</sub>O, H<sub>2</sub>CO and CH<sub>3</sub>OH are heavily fractionated. HDCO fractionation crossing unity for most of the time. We notice that during the late time (beyond  $10^6$  year), abundance of HDCO is enhanced over the abundance of H<sub>2</sub>CO. In Caselli et al. (2002b), it was assumed that activation barriers for the reactions such as H+CO ( $E_1$ ) and H+H<sub>2</sub>CO ( $E_2$ ) were in the range of 1000 – 2000 K. For the same

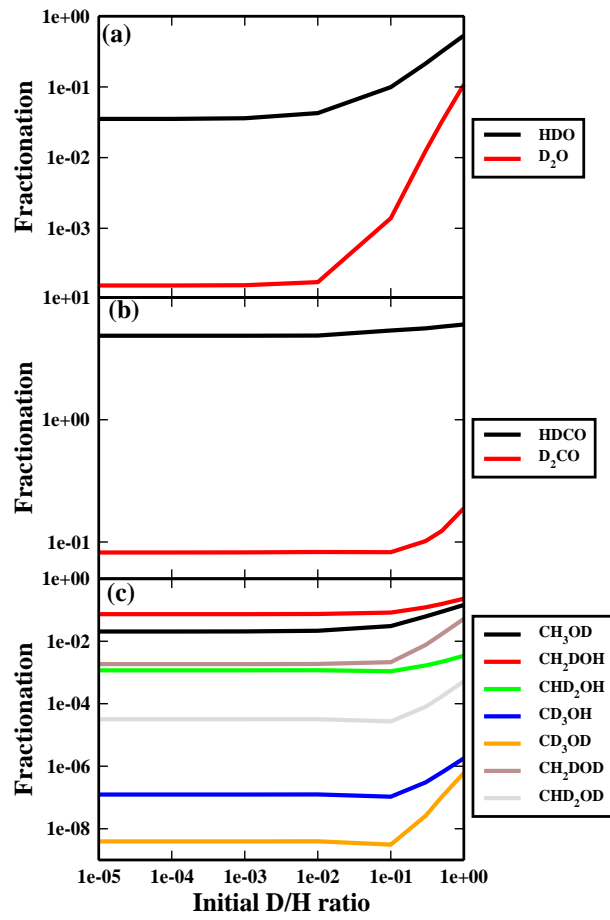


Figure 9: Deuterium fractionation of Ice phase (a) H<sub>2</sub>O, (b) H<sub>2</sub>CO and (c) CH<sub>3</sub>OH molecules.

reaction with deuterium, i.e., D+CO activation barrier differ slightly due to zero point vibrations. They assumed for the reaction D+CO, the barrier is  $E_1 - 70$  K. For reactions D+H<sub>2</sub>CO, H+HDCO, D+HDCO, H+D<sub>2</sub>CO and D+D<sub>2</sub>CO energy barriers were considered to be  $E_2 - 201$  K,  $E_2 - 35$  K,  $E_2 - 242$  K,  $E_2 - 75$  K and  $E_2 - 287$  K respectively. In this paper, unless otherwise stated, we used this consideration alone and assumed  $E_1 = E_2 = 2000$  K. Most recent findings by Fuchs et al. (2009), suggest that the energy barriers ( $E_1$  &  $E_2$ ) could be much lower than what was suggested by Caselli et al. (2002b). According to Fuchs et al. (2009), for the reaction H+CO, activation energy barrier is  $390 \pm 40$  K and for the reaction H+H<sub>2</sub>CO it is  $415 \pm 40$  K. In a test case, we have considered  $E_1 = 390$  K and  $E_2 = 415$  K respectively for H+CO and H+H<sub>2</sub>CO reactions. Keeping in mind the consideration of Caselli et al. (2002b), activation energy barriers for D+CO, D+H<sub>2</sub>CO, H+HDCO, D+HDCO, H+D<sub>2</sub>CO and D+D<sub>2</sub>CO reactions become 320 K, 214 K, 380 K, 173 K, 340 K and 128 K respectively. In reality, the difference in zero point vibrations should depend on the size of the barrier and for lower barriers these differences should be less. Here, we are considering the barrier energies which were considered by Caselli et al. (2002) and references therein. They assumed that for the reactions in which D atoms partially replace the H atoms have different activation energy barriers than  $E_1$  and  $E_2$  due to zero-point vibrations. These values were calculated by D. Woon (private communication), these differences are accurate, regardless of the accuracy of the barriers for the H + CO and H + H<sub>2</sub>CO reactions. According to Kaiser et al. (1999), ab-initio calculations show that isotopic substitution of H by D influences zero- point vibrational energy. Thus, differences in activation energy barriers for above reactions are obvious. Isotopic substitution can modify the rate of reactions in various ways. In many cases, differences can be rationalized by noting how the mass of an atom affects vibrational frequency of a chemical bond even if the electron configuration is nearly identical. Heavier atoms will (classically) lead to lower vibration frequencies, or, viewed quantum mechanically, will have lower zero-point energy. With a lower zero-point energy, more energy must be supplied to break the bond, resulting in a higher activation energy for bond cleavage, which in turn lowers the measured rate (Carten et al., 2011; Carten et al., 2012).

We ran our code for all these sets (set 1, set 2, set 3 and experimental activation barrier using set 1). To have an idea of how the results differ, in Table 3, we present fractionation ratios along with their respective column densities for initial atomic D/H ratio 0.1,  $n_H = 10^4$ ,  $T = 10$  K and  $A_V = 10$ . Moreover, in Table 3, we include the same for various energy values. Since for ice phase species, we reach a steady state during late stage of the evolution process, column densities and fractionation ratios are given in Table 3 during late stages (after the simulation time is over  $\sim 10^7$  year) of simulation.

### 3. Quantum Chemical Model

#### 3.1. Computational details

A significant amount of work is reported in the literature where spectroscopic investigation of different interstellar species is guided by theoretical predictions (e.g., Huang & Lee, 2008, 2009; Majumdar et al., 2013, 2014ab; Das et al., 2013a). Vibrational spectroscopy and rotational spectroscopy are widely used to identify several

species of interstellar interest. To compute vibrational (harmonic) frequencies, we optimize geometries of different deuterated neutrals and ions at density functional theory based on Becke three parameter Exchange and Lee, Yang and Parr correlation functional (B3LYP, Becke 1993, Lee, Yang & Parr, 1988) with 6-311++G basis set. We use B3LYP/6-311++G levels of theory for optimization of different interstellar species. Geometry optimization enabled us to locate minimum energy configuration of these deuterated species. This procedure calculates wave function and energy at a starting geometry and then proceeds to search for a new geometry of a lower energy. This is repeated until the lowest energy geometry of these species is found. The procedure calculates forces on each atom of species by evaluating gradient of energy with respect to atomic positions. Vibrational frequencies for all these species are also obtained at the same level of theory and these frequencies depend on second derivative of energy with respect to nuclear positions. To study chemical as well as spectroscopic properties of all neutral deuterated species in ice phase (water ice), we first optimize geometry of these species at B3LYP/6-311++G level with integral equation formalism variant (IEFPCM) as default self-consistent reaction field (SCRF) method with a dielectric constant of 78.5. SCRF calculation using IEFPCM model as implemented in Gaussian 09W (Frisch et al., 2009) program was used to include bulk solvation effect of medium as water ice. The IEFPCM bulk solvent medium is simulated as a continuum of dielectric constant ( $\epsilon = 78.5$ ), which surrounds a solute cavity defined by the union of a series of interlocking spheres centered on the atoms. For this computation, we optimize geometries of different neutral deuterated species at B3LYP/6-311++G level of theory of Gaussian 09W program with the polarizable continuum model and the integral equation formalism variant as a default SCRF method. These methods provide a proper ice phase environment for these neutral deuterated condensed phase species. Here, solute-solvent electrostatic interactions are treated at dipole level. Solvent effect brings significant changes in geometrical parameters of these condensed phase deuterated species. Our model confirms that polarization of the solute by continuum has important effects on absolute and relative solvation energies, which, in turn shift frequency as compared to gas phase.

To the best of our knowledge, no detailed investigation has been carried out for computation of different rotational and centrifugal-distortional constants for different deuterated interstellar neutral and ions simultaneously. Usually, these constants are evaluated at the same level as corresponding force fields needed either for prediction of vibrational frequencies or vibrational corrections to rotational constants. Here, we use MP2/6-311++G(d,p) level of theory for performing our calculations. Corrections for interaction between rotational motion and vibrational motion along with corrections for vibrational averaging and anharmonic corrections to vibrational motion are also considered in our calculations. In brief, we report here rotational and distortional constants of all important neutral and ionic deuterated species in our model, which are corrected for each vibrational state as well as vibrationally averaged structures. These rotational constants are required to predict different rotational transitions and this can be done using the ‘SPCAT’ program (Pickett, 1991).

### 3.2. Results of Quantum chemical modeling

Several gas phase deuterated molecules are observed till date mostly by observing rotational transitions. We carried out quantum chemical calculations by using the method described in section 3.1.

A complex pattern of chemical change could be visible due to collapse of a dense cloud core leading to the formation of a young star and its circumstellar disk. Processes such as depletion of molecules on cold icy grains during collapsing phase, evaporation of newly-formed species when a protostar starts to heat its surroundings, and high temperature reactions in shocked zones created by impacts of outflow, cycle molecules from one compound into another. These changes are not only of chemical interest, but can also be used as diagnostics of physical state of evolution of an object. Moreover, knowledge of chemistry is needed to choose proper molecular line to trace physical structure of a particular component. In single-dish observations with 15'' – 30'' beams, all of these different chemical processes are blurred together, whereas current interferometers with a few arcsec resolution suffer from poor spatial sampling. ALMA, with its unprecedented sensitivity, resolution and UV coverage will be necessary to zoom in and image these different chemical regimes and quantitatively address chemical evolution in the initial stages of star formation. Due to this reason, we concentrate only on 3 to 9 (84 – 720GHz) band of ALMA. In order to assist observational identifications, in Table 4, we provide different rotational parameters for the most important neutral gas phase deuterated species. These rotational parameters are necessary to predict spectrum of these species (Pickett, 1991). Among different neutral deuterated species in Table 4, DNC and DCN are linear molecules. In order to get all rotational parameters for these species, we need to apply degenerate perturbation theory to correctly compute bending modes of these species. But as this feature is not implemented in Gaussian 09W program, we obtain only single rotational constant (B) for DCN and DNC. Moreover, some rotational transitions which are falling in 84 – 720GHz (bands 3 – 9 of ALMA) range, are also given in Table 5. Column density of deuterated species are calculated by using the following relation used by Shalabiea et al. (1994), Das & Chakrabarti (2011) and Das et al. (2013a).

$$N(A) = n_H x_i R,$$

where,  $n_H$  is the total hydrogen number density,  $x_i$  is the abundance of  $i^{th}$  species and  $R$  is path length along the line of sight ( $= 1.6 \times 10^{21} A_V / n_H$ ). Peak column density of all the neutral deuterated species are presented in Table 5. Observed column densities are also given with corresponding references. Peak values of ice phase column densities are tabulated along with gas phase column densities. In case of formaldehyde and methanol, our calculated gas phase column densities differ by some orders of magnitudes from the observed values. Our calculated ice phase column densities might be a clue for this. For example, as per Loinard et al. (2000), observed column density of HDCO varies between  $4.8 \times 10^{13} - 8.1 \times 10^{13} \text{ cm}^{-2}$ . Our calculated peak value of the gas phase HDCO is  $3.23 \times 10^8 \text{ cm}^{-2}$ . But peak value of calculated ice phase column density is  $6.48 \times 10^{15}$  which indicates that these types of species are mainly synthesized on dust surfaces at low temperature and could populate gas phase subsequently via some energetic events (stellar ejecta, in hot cores associated with proto-stars, in dense photo-dissociation regions associated with luminous stars, or in the post-shock regions). So,

HDCO could be produced during the cold phase of the molecular cloud but when the surrounding cloud become warmer (by some energetic events), ice would sublime and release all the species in the gas phase. We compare our theoretically computed transitions with earlier works and find that some of the transitions match exactly. Calculated column density of deuterated isotopomers of methanol and  $\text{H}_2\text{CO}$  are found to be very low. These molecules could efficiently be formed on grain surfaces and could populate the gas phase by some energetic events.

As in the case of gas phase neutral deuterated species, here also different rotational and distortional constants for deuterated ions are given in Table 6. To obtain all rotational and distortional constants for linear molecules, such as  $\text{DCO}^+$ ,  $\text{DCN}^+$ ,  $\text{CD}^+$  and  $\text{N}_2\text{D}^+$ , it is necessary to use degenerate perturbation theory which could correctly account for bending modes. But this feature is not implemented in GAUSSIAN 09W program. That is why we tabulate only 'B' value for these species. Peak column densities of these gas phase deuterated ions along with its possible rotational transitions only in the range of 84 – 720GHz are presented in Table 6. A comparison with our computed transitions are also highlighted in Table 7.

In order to describe inconsistencies between transitions reported in this work and other catalogs (JPL, NIST), we would like to mention that first step towards observation of new molecules in an ISM is to obtain transition frequencies. For this, rotational and distortional constants have to be calculated using a suitable method. Hence it is always important and advantageous to have a good frequency prediction before an experiment or observation as spectrometers do not generally have automated scanning mode. This significantly reduce manual scanning time in high resolution spectroscopic observations. Rotational and distortional constants can be calculated using two methods, namely, by computational quantum chemistry and experiments. In order to measure experimental rotational spectra of different species at temperatures around 10 K or less (interstellar environment), one can use cavity Fourier transform, chirped pulse or with free jets, stark modulation spectrometers etc. Millimeter wave (30 – 300 GHz) and sub-millimeter wave (300 – 3000 GHz) rotational spectra are most efficiently obtained in frequency domain with broad-band spectrometers. Expected resolution of the rotational spectrum is determined by Doppler limited line widths of absorption lines but sometimes also by experimental techniques used for the detection. Now, most of rotational and distortional constants in a catalogs are reported by fitting (using the SPFIT program package written by H. M. Pickett of JPL) observed experimental transitions (using the above methods) with selected Hamiltonian. SPFIT program provides extended possibilities for definition of molecular Hamiltonian required for a particular problem. This program also allows declaration of spectroscopic parameters for all type of rotors. The fitting program produces an input file with improved spectroscopic constants for use of SPCAT program to calculate the spectra. Computational chemistry has greatly enhanced predictive power for such experiments and observations. For most of the molecular system, exact solution of the Schrödinger equation are not possible. Molecular system that are studied here ranges from neutral deuterated to ionic deuterated species. The smallest neutral system studied in this work is HDO with 3 atoms and 11 electrons. *Ab initio* method MP2 was used in this work which scale as  $N^5$  in computational time with the number of electrons. This method is proven to be accurate as compared to other available methods (Das et al., 2013a; Majumdar et al.,

2014a; Majumdar et al., 2014b). The goal of calculations performed prior to an experiment is to generate coordinates for the nuclei in a molecule. Moment of inertia can be obtained from coordinates of atoms and masses. First, center of mass is determined and coordinates are then generated from origins placed at the center of mass. The principle axes of the system can be determined by diagonalizing moment of inertia matrix. Once moment of inertia is determined for the principle axis, rotational constants can be determined. Symmetric and asymmetric top spectra are known combinations of rotational constants. The SPCAT program then can be used to generate spectrum and transitions from rotational and distortional constants. This prediction will be the starting point for all the molecules reported in this work.

Majumdar et al. (2014a) reported rotational and distortional constants for  $\text{CH}_2\text{CN}^-$ ,  $\text{CHDCN}^-$  and  $\text{CD}_2\text{CN}^-$  in symmetrically reduced Hamiltonian. Experimental values of these constants were available for  $\text{CH}_2\text{CN}^-$  and  $\text{CD}_2\text{CN}^-$  by fitting observed experimental transitions with Watson S-reduced Hamiltonian using a least square routine (Lykke et al., 1987). Majumdar et al. (2014a) mentioned that errors on computed line frequencies are related to errors on calculated rotational and distortional constants. There were some uncertainties from experimentally obtained values as well. From there, Majumdar et al. (2014a) pointed out that these uncertainties could result in an error in between 0.6MHz and 12MHz for frequency range in between 18GHz and 319GHz. Higher uncertainty was associated with higher frequencies. Here, we observe a similar situation. Tables 5 and 7 clearly show that our results are in agreement at lower frequencies ( $< 200\text{GHz}$ ). Our predicted frequencies for deuterated formaldehyde and methanol are within the error bar of 2 GHz for transitions below 300 GHz. In case of  $\text{D}_2\text{CO}$ , our calculated transition for  $4_{04} \rightarrow 3_{03}$  is at 231.988 GHz whereas in JPL catalog this transition is tabulated at 231.41021 GHz, so the error bar is 0.578 GHz. In case of  $\text{CH}_2\text{DOH}$  our calculated transition for  $2_{02} \rightarrow 1_{01}$  is at 89.80 GHz whereas in JPL catalog this transition is pointed out at 89.25 GHz and for  $\text{CH}_3\text{OD}$  our calculated transition for  $2_{02} \rightarrow 1_{01}$  is at 91.3 GHz whereas in JPL catalog this transition is pointed out at 90.703 GHz. In JPL or NIST, no frequencies for our given transitions are presented for  $\text{CH}_2\text{DOD}$ ,  $\text{CHD}_2\text{OD}$ ,  $\text{CD}_3\text{OD}$ . Since our computed transitions for singly and doubly deuterated methanols are in good agreement for the lower frequency range ( $< 300\text{GHz}$ ), we hope our computed frequencies will be helpful to detect  $\text{CH}_2\text{DOD}$ ,  $\text{CHD}_2\text{OD}$ ,  $\text{CD}_3\text{OD}$  in the ISM. These frequencies along with our computed column densities could be used to predict the source antenna temperature by using CASSIS interactive spectrum analyzer (Caux et al., 2011). Now to convert the antenna temperature to the source flux density, following relation could be used:

$$S_\nu = 3520 \times \frac{T_a}{\eta_A D^2},$$

where,  $\eta_A$  is the aperture efficiency and  $D$  is the diameter. By including all the values, one could have the source flux density ( $S_\nu$ ). This information would be extremely helpful for the observer for the detection of these species in the ISM.

Theoretical prediction of rotational and distortional constants depends on various choices (Bowman et al., 2007; Carter et al., 2009): i. Choice of ab initio potentials (depend on degrees of freedom), ii. Choice of ab initio dipole moment surface, iii. Development of essential quantum methods to calculate rovibrational wave functions.

First of all, it is very time consuming and each species requires different quantum chemical treatments. Computational studies could be feasible for smaller molecular species, extensions to larger molecular systems with various variable (e.g. mass, charge for ions etc.) remain a computational challenge. Currently, full spectral treatment for molecules having more than few atoms is limited to the use of effective Hamiltonians, which often do not provide results close to observations or experiments (Carter et al., 2011, 2012). Theoretical computed spectral line-lists provide an essential complement to experimentally measured ones. One obvious way that theory can complement experiment is in filling in the gaps in laboratory-measurements. Theoretical line-lists can in principle span the entire spectral range.

In earlier Section, it was pointed out that various deuterated molecules could be trapped inside an interstellar ice. Existence of deuterated isotopomers in interstellar ice analogues could be traced by observing through IR telescopes. In order to assist observers, we calculate vibrational frequencies for various deuterated isotopomers. For this computation, we optimize geometries of molecules by density functional theory based on B3LYP method and 6-311++G basis set of GAUSSIAN 09W program. In Table 8, IR features of various ice phase isotopomers of Water,  $\text{H}_2\text{CO}$  and  $\text{CH}_3\text{OH}$  are given. We have also tabulated gas phase IR features of these isotopomers to highlight spectral changes due to isotopic substitution. In Table 9, we provide IR features of gas phase deuterated ions. Only for representation, in Fig. 10a and Fig. 10b, we show IR spectra of gas phase  $\text{DCO}^+$ ,  $\text{HCO}^+$ ,  $\text{N}_2\text{D}^+$  and  $\text{N}_2\text{H}^+$  respectively. This Figure explains that isotopic substitution plays a dominant role in IR spectral features.

#### 4. Conclusions

Despite a low elemental abundance of atomic deuterium in interstellar space, some species are observed to be heavily fractionated by deuterium. Sometimes fractionation ratio crosses observed elemental D/H ratio ( $\sim 1.5 \times 10^{-5}$ ). In order to find out evolution history of deuterated species, we make use of a large gas-grain chemical network. We applied our model for mimicking cold dark cloud region of an ISM. Moreover, we have also performed quantum chemical simulation to compute several spectral parameters which could encourage observers for further investigation of deuterated species in and around an ISM. In brief, followings are the highlights of the present work:

- Chemical evolutions of deuterated molecules in gas and ice phases are discussed. Computed abundances of gas phase deuterated isotopomers of formaldehyde and some isotopomers of methanol are found to be below present observational limits. However, their abundances in ice phase are reasonable. We hope that these ice phase molecules could populate the gas phase by some energetic events making them detectable.
- Column densities of deuterated species are computed and are compared with observed column densities.
- Rotational and distortion constants for some of the important deuterated species are computed by quantum chemical simulations.
- Rotational and vibrational (harmonic) spectral transitions are calculated for some of the abundant deuterated species and are compared with other theoretical, observational or experimental databases.



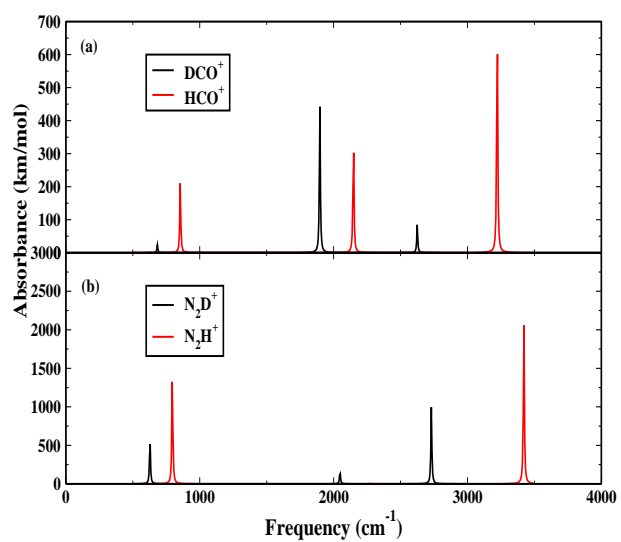


Figure 10: IR spectra of gas phase (a) HCO<sup>+</sup> and DCO<sup>+</sup> and (b) N<sub>2</sub>H<sup>+</sup> and N<sub>2</sub>D<sup>+</sup>.

- Dependences of deuterium fractionation of ice phase species for different binding energies and activation energy barriers are discussed.
- Various regions of a collapsing cloud are modeled and radial distribution of  $R_1$  ( $\text{DCO}^+/\text{HCO}^+$ ) and  $R_2$  ( $\text{N}_2\text{D}^+/\text{N}_2\text{H}^+$ ) is studied.

#### 4.1. Acknowledgments

AD and DS are grateful to ISRO for financial support through a respond project (Grant No. ISRO/RES/2/372/11-12), SKC acknowledges a DST project (Grant No. SR/S2/HEP-40/2008) for partial financial support and LM thanks MOES project for his partial financial support. Authors would like to thank an anonymous referee whose valuable suggestions helped to improve this paper significantly.

#### References

- [1] Aikawa, Y., Herbst, E., Roberts, H., Caselli, P., 2005, ApJ 620, 330.
- [2] Akai, Y., Saito, S. 2003, Jpn. J. Appl. Phys., 42, 640
- [3] Albertsson, T., Semenov, D. A., Vasyunin, A. I., Henning, T., Herbst, E. 2013, ApJS, 207, 27
- [4] Allen, M., Robinson, G. W., 1977., ApJ, 212, 396
- [5] André, P., Ward-Thompson, D., Barsony, M. 1993, ApJ, 406, 122
- [6] Bacmann, A., Lefloch, B., Ceccarelli, C., Steinacker, J., Castets, A., Loinard, L., 2003, ApJ, 585
- [7] Bergman, P., Parise, B., Liseau, R., Larsson, B., 2011, A&A, 527, 39
- [8] Bergeron, H., Rougeau, N., Sidis, V., et al. 2008, J. Phys. Chem. A, 112, 11921
- [9] Bowman, J. M., Huang, X., Handy, N. C., Carter, S. 2007, J. Phys. Chem. A 111, 7317
- [10] Snow, T. P., McCal. B. J. 2006, ARA&A, 44, 367
- [11] Butner, H. M., Lada, E. A., Loren, R. B., 1995, ApJ, 448, 207
- [12] Becke A. D., 1993, J. Chem. Phys., 98, 5648
- [13] Caux Caux, E., Kahane, C., Castets, A. et al. 2011, A&A, 532, A23
- [14] Carter, S., Sharma, A. R., Bowman, J. M. 2012, J. Chem. Phys. 137, 154301
- [15] Carter, S., Sharma, A. R., Bowman, J. M. 2011, J. Chem. Phys. 135, 014308.
- [16] Coutens, A., Vastel, C., Cazaux, S., Bottinelli, S., Caux, E., Ceccarelli, Demyk, K., Taquet, V., Wakelam, V., 2013, A&A, 553, 75
- [17] Caselli, P., 2002, P&SS, 50, 1133
- [18] Caselli, P., Stantcheva, T., Shalabiea, O., Shematovich, V. I. & Herbst, E., 2002, P&SS, 50, 1257
- [19] Caselli, P., Vastel, C., Ceccarelli, C., Van der Tak, F. F. S., Crapsi, A., Bacmann, A., 2008, A&A, 492, 703
- [20] Cazaux, S., Cobut, V., Marseille, M., Spaans, M., Caselli, P. 2010, A&A, 522, 74
- [21] Coutens, A., Vastel, C., Caux, E., et al. 2012, A&A, 539, A132
- [22] Coutens, A., Vastel, C., Cazaux, S., et al. 2013, A&A, 553, A75
- [23] Coutens, A., Vastel, C., Cabrit, S. et al. 2013, A&A, 560A, 39
- [24] Cuppen, H. M., Herbst, E., 2007, APJ, 668, 294
- [25] Chakrabarti, S., Chakrabarti, S. K., 2000a, A&A 354, L6
- [26] Chakrabarti, S. K., Chakrabarti, S., 2000b, Ind. J. Phys 74B, 97
- [27] Chakrabarti, S. K., Das, A., Acharyya, K., Chakrabarti, S., 2006, A&A, 457, 167
- [28] Chakrabarti, S. K., Das, A., Acharyya, K., Chakrabarti, S., 2006, BASI, 34, 299
- [29] Ceccarelli, C., Castets, C., Loinard, L., Caux, E., Tielens, A. G. G. M., 1998, A&A, 338, L43
- [30] Crapsi, A., Caselli, P., Walmsley, C. M., Myers, P. C., Tafalla, M., Lee, C. W., Bourke, T. L., 2005, ApJ, 619
- [31] Das, A., Acharyya, K., Chakrabarti, S. & Chakrabarti, S. K., 2008a, A&A, 486, 209
- [32] Das, A., Chakrabarti, S. K., Acharyya K. & Chakrabarti, S., 2008b, NEWA, 13, 457
- [33] Das, A., Acharyya, K. & Chakrabarti, S. K., 2010, MNRAS 409, 789

- [34] Das, A. & Chakrabarti, S. K., 2011, 418, 545, MNRAS
- [35] Das, A. Majumdar, L., Chakrabarti, S. K., & Chakrabarti S., 2013, MNRAS, 433, 3152
- [36] Das, A. Majumdar, L., Chakrabarti, S. K., & Chakrabarti S., 2013, New Astronomy, 23, 118
- [37] Emprechtinger, M., Caselli, P., Volgenau, N. H., Stutzki, J., Wiedner, M. C., 2008, A&A, 493, 89
- [38] Frisch, M. J.; Trucks, G. W.; Schlegel, H. B., et al. 2009, Gaussian 09, Revision D.01, D. J. Gaussian, Inc., Wallingford CT
- [39] Froebrich, D. 2005, ApJS, 156, 169
- [40] Garrod, R. T., Wakelam, V. and Herbst, E., 2007, A&A, 467, 1103
- [41] Ghio, E., Mattera, L., Salvo, C., Tommasini, F., Valbusa, U. 1980, J. Chem. Phys., 73, 556
- [42] Hasegawa, T., Herbst, E., Leung, C.M., 1992, APJ, 82, 167
- [43] Hasegawa, T., Herbst, E., 1993, MNRAS, 261, 83
- [44] Huang, X., Lee, T. J. 2008, JChPh, 129, 044312
- [45] Huang, X., Lee, T. J. 2009, JChPh, 131, 104301
- [46] Jørgensen, J. K., Schier, F. L., van Dishoeck, E. F. 2004, A&A, 416, 603
- [47] Kaiser R. L., Ochsenfeld C., Head-Gordon M., Lee Y. T., 1999, ApJ, 510, 784
- [48] Katz, N., Furmann, I., Biham, O., Pironello, V. and Vidali, G., 1999, ApJ 522, 305
- [49] Kroes, G. J., Andersson, S. 2006, IAU Symp., 231, 427
- [50] Lada, C. J., Wilking, B. A. 1984, ApJ, 287, 610
- [51] Lee, H. H., Herbst, E., Forets, G. P., Roueff, E., Bourlot, J. L., 1996, A&A, 311, 690
- [52] Lee C., Yang W., Parr R. G., 1988, Phys. Rev. B, 58, 785
- [Leger et al. 1985] Leger, A., Jura, M., Omont, A., 1985, A&A, 144, 147
- [Linsky et al. 1995] Linsky, J.L., Diplas, A., Wood, B.E., Brown, A., Ayres, T.R., Savage, B.D., 1995, ApJ, 451, 335, B351.
- [55] Loinard, L., Castets, A., Ceccarelli, C., Tielens, A. G. G. M., Faure, A., Caux, E., Duvert, G., 2000, A&A, 359, 1169
- [56] Looney, L. W., Mundy, L. G., Welch, W. J., 2003, ApJ, 592, 255
- [57] Majumdar, L., Das, A., Chakrabarti, S.K., 2014, A&A, 562, A56
- [58] Majumdar, L., Das, A., Chakrabarti, S.K., 2014, ApJ, 782, 73
- [59] Majumdar, L., Das, A., Chakrabarti, S.K., Chakrabarti, S., 2013, New Astronomy, 20, 15
- [60] Majumdar, L., Das, A., Chakrabarti, S.K., Chakrabarti, S., 2012, Research in Astronomy & Astrophysics, 12, 1613
- [61] Miettinen, O., Harju, J., Haikala, L. K., Juvola, M., 2012, A&A, 538, 137
- [62] Muller, H. S. P., Schloder, F., Stutzki, J., Winnewisser, G. 2005, JMoSt, 742, 215
- [63] Muller, H. S. P., Thorwirth, S., Roth, D. A., Winnewisser, G. 2001, A&A, 370, L49
- [64] Myers, P. C., Adams, F. C., Chen, H., et al. 1998, ApJ, 492, 703
- [65] Neill, J. L., Wang, S., Bergin, E. A., Crockett, N. R., Favre, C., Plume, R., Melnick, G. J., 2013, ApJ, 770, 142
- [66] Noble, J. A., Theule, P., Mispelaer, F., Duvernay, F., Danger, G., Congiu, E., Dulieu, F., Chiavassa, T., 2012, A&A, 543, A5
- [67] Dulieu, F., Congiu, E., Noble, J. et al., 2013, Nature, 3E, 1338
- [68] Pilling, M. J. 2006, in Faraday Discussions, Chemical Evolution of the Universe, 133, 97
- [69] Pirronello, V., Biham, O., Liu, C., Shena, L. and Vidali, G., 1997, ApJ, 483L, 131
- [70] Pirronello, V., Liu, C., Riser, J.E. and Vidali, G., 1999, A&A, 344, 681
- [71] Pickett, H. M., J. Mol. Spectrosc., 1991, 148, 371
- [72] Parise, B., Ceccarelli, C., Tielens, A. G. G. M., Herbst, E., Leach, B., Caux, E., Castets, A., Mukhopadhyay, I., Pagani, L., Loinard, L., 2002, A&A, 393, L49
- [73] Parise, B., Castets, A., Herbst, E., Caux E., Ceccarelli, C., Mukhopadhyay, I., Tielens, A.G.G.M, 2004, A&A, 416, 159
- [74] Parise, B., Caux, E., Castets, A., et al. 2005, A&A, 431, 547
- [75] Parise, B., Leurini, S., Schilke, P., Roueff, E., Thorwirth, S., Lis, D. C., 2009, A&A, 508, 737

- [76] Parise, B., Ceccarelli, C., Tielens, A.G.G.M., Castets, A., Caux, E., Leach B.,  
Maret, S., 2006, A&A, 453, 949
- [77] Persson, M. V., Jrgensen, J. K., van Dishoeck, E. F. 2013, A&A, 549, L3
- [78] Roberts, H., Millar, T. J., 2000, A&A, 361, 388
- [79] Roberts, H., Herbst, E., Millar, T. J., 2002, MNRAS, 336, 283
- [80] Roberts, H., Herbst, E., Millar, T. J. 2003, ApJ, 591, L41
- [81] Rodgers, S. D., Millar, T. J., 1996, MNRAS, 280, 1046 A&A, 438,585
- [82] Serrallach, A., Meyer, R., Gunthard, Hs. H., 1974, J. Mol. Spec., 52, 94
- [83] Shu, F. H., 1977, ApJ, 214, 488
- [84] Smith, M. 1998, Ap&SS, 261, 169
- [85] Stantcheva, T., Shematovich, V. I., Herbst, E., 2002, A&A, 391, 1069
- [86] Tielens, A. G. G. M., Allamandola, L. J., 1987, in Interstellar Process, ed. D. J.  
Hollenbach & H. A. Thronson, Jr. (Dordrecht:Kluwer), 397
- [87] Turner, B.E., 1990, 362, L29
- [88] Watson, W. D., 1976, Rev. Mod. Phys., 48, 513
- [89] Woodall, J., Agn dez, M., Markwick-Kemper, A.J., Millar, T.J., 2007, A&A, 466,  
1197

Table 4: Rotational and distortional constants for different neutral deuterated species at MP2/6-311G++(d,p) level of theory

Gas phase deuterated species	Rotational constants	Calculated Values (in MHz)	Distortional constants	Calculated Values (in MHz)
<b>HDO</b>	A B C	678940.54787 275198.74337 195714.67931	$D_J$ $D_{JK}$ $D_K$ $d_1$ $d_2$	$0.1086365352 \times 10^2$ $-0.3895959732 \times 10^2$ $0.5654979144 \times 10^3$ $-0.3994210593 \times 10^1$ $-0.3131595732 \times 10^0$
<b>D<sub>2</sub>O</b>	A B C	445056.83172 221168.53834 147688.78486	$D_J$ $D_{JK}$ $D_K$ $d_1$ $d_2$	$0.9060508212 \times 10^1$ $-0.4308532587 \times 10^2$ $0.2230651871 \times 10^3$ $-0.3754958073 \times 10^1$ $-0.1506205890 \times 10^0$
<b>DCN</b>	A B C	- 35437.934 -	$D_J$ $D_{JK}$ $D_K$ $d_1$ $d_2$	- - - - -
<b>DNC</b>	A B C	- 37466.722 -	$D_J$ $D_{JK}$ $D_K$ $d_1$ $d_2$	- - - - -
<b>HDCO</b>	A B C	199693.34999 34528.56786 29437.69695	$D_J$ $D_{JK}$ $D_K$ $d_1$ $d_2$	$0.5328503572 \times 10^{-1}$ $0.1028419257 \times 10^1$ $0.8917367749 \times 10^1$ $-0.9570179851 \times 10^{-2}$ $-0.2627217258 \times 10^{-2}$
<b>D<sub>2</sub>CO</b>	A B C	142634.08807 31918.80631 26081.57265	$D_J$ $D_{JK}$ $D_K$ $d_1$ $d_2$	$0.4362335359 \times 10^{-1}$ $0.6360353879 \times 10^0$ $0.414917034 \times 10^1$ $-0.1031801248 \times 10^{-1}$ $-0.2978222074 \times 10^{-2}$
<b>CH<sub>3</sub>OD</b>	A B C	110017.71408 23551.47123 22129.23533	$D_J$ $D_{JK}$ $D_K$ $d_1$ $d_2$	$0.4614264313 \times 10^{-1}$ $0.2163668137 \times 10^0$ $0.8855341581 \times 10^0$ $-0.2682781206 \times 10^{-2}$ $0.2173182807 \times 10^{-2}$
<b>CH<sub>2</sub>DOH</b>	A B C	102649.07681 22889.94059 22010.93836	$D_J$ $D_{JK}$ $D_K$ $d_1$ $d_2$	$0.4204194260 \times 10^{-1}$ $0.2750167913 \times 10^0$ $0.6689263671 \times 10^0$ $-0.1443976902 \times 10^{-2}$ $0.1103933246 \times 10^{-2}$
<b>CHD<sub>2</sub>OH</b>	A B C	84155.94541 21068.30406 20719.18545	$D_J$ $D_{JK}$ $D_K$ $d_1$ $d_2$	$0.3517956906 \times 10^{-1}$ $0.2322462933 \times 10^0$ $0.3896941170 \times 10^0$ $-0.7434073238 \times 10^{-3}$ $0.9511728787 \times 10^{-3}$
<b>CD<sub>3</sub>OH</b>	A B C	70831.43728 19919.38820 19371.86590	$D_J$ $D_{JK}$ $D_K$ $d_1$ $d_2$	$0.2940531648 \times 10^{-1}$ $0.1586623951 \times 10^0$ $0.2625638578 \times 10^0$ $-0.6736522611 \times 10^{-3}$ $0.5710887562 \times 10^{-3}$
<b>CH<sub>2</sub>DOD</b>	A B C	90311.79171 21697.63492 22129.23533	$D_J$ $D_{JK}$ $D_K$ $d_1$ $d_2$	$0.3992772304 \times 10^{-1}$ $0.1966259292 \times 10^0$ $0.5493414294 \times 10^0$ $-0.2225437219 \times 10^{-2}$ $0.2323808569 \times 10^{-2}$
<b>CHD<sub>2</sub>OD</b>	A B C	75426.27536 19810.90663 19611.52641	$D_J$ $D_{JK}$ $D_K$ $d_1$ $d_2$	$0.3428624222 \times 10^{-1}$ $0.1734390959 \times 10^0$ $0.3206028770 \times 10^0$ $-0.4950184016 \times 10^{-3}$ $0.2378618627 \times 10^{-2}$
<b>CD<sub>3</sub>OD</b>	A B C	64997.04836 18968.64086 18049.58590	$D_J$ $D_{JK}$ $D_K$ $d_1$ $d_2$	$0.2737158018 \times 10^{-1}$ $0.1232098414 \times 10^0$ $0.2124252221 \times 10^0$ $-0.1279839822 \times 10^{-2}$ $0.1339069324 \times 10^{-2}$

Table 5: Calculated and observed rotational transitions of some neutral gas phase deuterated species

Neutral deuterated species	Gas phase/Ice phase Column density (in $\text{cm}^{-2}$ )	Observed/estimated column density (in $\text{cm}^{-2}$ )	Transitions	Calculated frequency (in GHz)	Comparison with (Observation/Theory)
<b>HDO</b>	$1.19 \times 10^{15} / 1.62 \times 10^{17}$	$4.4 \times 10^{13 p9}$	$1_{01}-0_{00}$ $2_{02}-1_{01}$	470.854 941.432	$464.924^{ni}$ $919.3109^{n,j}$
<b>D<sub>2</sub>O</b>	$1.13 \times 10^{14} / 2.26 \times 10^{15}$	$2.5 \times 10^{12 c}$	$1_{01}-0_{00}$ $2_{02}-1_{01}$	368.807 737.390	
<b>DCN</b>	$1.78 \times 10^{16} / 2.08 \times 10^{16}$	$1.4 \pm 0.3 \times 10^{13 p9}$	$2_{02}-1_{01}$ $3_{03}-2_{02}$ $4_{04}-3_{03}$ $5_{05}-4_{04}$ $6_{06}-5_{05}$ $7_{07}-6_{06}$ $8_{08}-7_{07}$ $9_{09}-8_{08}$	141.753 212.629 283.505 354.381 425.256 496.132 567.008 637.884	$144.8280015^{p9}$ $217.2385378^{p9}$ $289.6449170^{p9}$ $362.0457535^{p9}$
<b>DNC</b>	$2.22 \times 10^{16} / 4.89 \times 10^{16}$	$1.5 \times 10^{11 p9}$	$1_{01}-0_{00}$ $2_{02}-1_{01}$ $3_{03}-2_{02}$ $4_{04}-3_{03}$ $5_{05}-4_{04}$ $6_{06}-5_{05}$ $7_{07}-6_{06}$ $8_{08}-7_{07}$ $9_{09}-8_{08}$	74.933 149.867 224.800 299.734 374.667 449.600 524.534 599.467 674.401	$152.609774^{p9}$
<b>HDCO</b>	$1.07 \times 10^8 / 1.87 \times 10^{15}$	$4.8 - 8.1 \times 10^{13 l}$	$2_{02}-1_{01}$ $3_{03}-2_{02}$ $4_{04}-3_{03}$ $6_{06}-5_{05}$ $7_{07}-6_{06}$ $8_{08}-7_{07}$ $9_{09}-8_{08}$	127.93 191.892 255.850 383.746 447.683 511.610 575.525	$128.813^{h,j}$ $192.893^j$ $256.586^{h,j}$ $382.342^j$ $444.227^j$ $505.391^j$ $565.850^j$
<b>D<sub>2</sub>CO</b>	$1.53 \times 10^7 / 2.42 \times 10^{13}$	$1.9 - 5 \times 10^{13 l}$	$2_{02}-1_{01}$ $3_{03}-2_{02}$ $4_{04}-3_{03}$ $5_{05}-4_{04}$ $6_{06}-5_{05}$ $7_{07}-6_{06}$ $8_{08}-7_{07}$ $9_{09}-8_{08}$	115.999 173.995 231.988 289.977 347.959 405.934 463.901 521.858	$116.68847^t, j$ $174.413^{h,j}$ $231.41021^t, j$ $287.486^{h,j}$ $342.52181^t, 342.522^c, j$ $396.517^j$ $449.596^j$ $501.983^j$
<b>CH<sub>3</sub>OD</b>	$7.70 \times 10^{13} / 1.11 \times 10^{16}$	$1.5 \pm 0.7 \times 10^{14 p4}$	$2_{02}-1_{01}$ $3_{03}-2_{02}$ $4_{04}-3_{03}$ $5_{05}-4_{04}$ $6_{06}-5_{05}$ $7_{07}-6_{06}$ $8_{08}-7_{07}$ $9_{09}-8_{08}$	91.3 137.037 182.712 228.382 274.048 319.707 365.360 411.004	$90.703^{ni}$ $136.026^{ni}$ $226.539^{p2,ni}$
<b>CH<sub>2</sub>DOH</b>	$1.51 \times 10^{14} / 2.98 \times 10^{16}$	$3.0 \pm 0.6 \times 10^{15 p4}$	$2_{02}-1_{01}$ $3_{03}-2_{02}$ $4_{04}-3_{03}$ $5_{05}-4_{04}$ $6_{06}-5_{05}$ $7_{07}-6_{06}$ $8_{08}-7_{07}$ $9_{09}-8_{08}$	89.80 134.698 179.593 224.484 269.370 314.251 359.125 403.991	$89.4^{p2}89.25^j$ $134.112^{p2}, 133.847^j$ $178.342^j$ $223.422^{p2}, 222.741^j$ $267.634^j$ $311.211^j$ $355.292^j$ $399.295^j$
<b>CHD<sub>2</sub>OH</b>	$2.71 \times 10^{12} / 3.94 \times 10^{14}$	$6.0 \pm 2.2 \times 10^{14 p4}$	$2_{02}-1_{01}$ $3_{03}-2_{02}$ $4_{04}-3_{03}$ $5_{05}-4_{04}$ $6_{06}-5_{05}$ $7_{07}-6_{06}$ $8_{08}-7_{07}$ $9_{09}-8_{08}$	83.573 125.358 167.141 208.920 250.696 292.466 334.231 375.990	$83.3^{p2}, 83.129^{ni}$ $166.23^{ni}$ $207.869^{p2}, 207.77^{ni}$
<b>CD<sub>3</sub>OH</b>	$3.30 \times 10^8 / 3.82 \times 10^{10}$	$7.30 \pm 2.3 \times 10^{13 p4}$	$2_{02}-1_{01}$ $3_{03}-2_{02}$ $4_{04}-3_{03}$ $5_{05}-4_{04}$ $6_{06}-5_{05}$ $7_{07}-6_{06}$ $8_{08}-7_{07}$ $9_{09}-8_{08}$	78.581 117.870 157.157 196.442 235.723 275.000 314.272 353.539	$156.242^{p6,ni}$

Neutral deuterated species	Gas phase Column density (in $\text{cm}^{-2}$ )	Observed/estimated column density (in $\text{cm}^{-2}$ )	Tansitions	Calculated frequency (in GHz)	Comparison with (Observation/Theory)
<b>CH<sub>2</sub>DOD</b>	$5.71 \times 10^{12} / 7.73 \times 10^{14}$		<sup>2</sup> <sub>02</sub> -1 <sub>01</sub> <sup>3</sup> <sub>03</sub> -2 <sub>02</sub> <sup>4</sup> <sub>04</sub> -3 <sub>03</sub> <sup>5</sup> <sub>05</sub> -4 <sub>04</sub> <sup>6</sup> <sub>06</sub> -5 <sub>05</sub> <sup>7</sup> <sub>07</sub> -6 <sub>06</sub> <sup>8</sup> <sub>08</sub> -7 <sub>07</sub> <sup>9</sup> <sub>09</sub> -8 <sub>08</sub>	84.512 126.766 169.018 211.266 253.510 295.749 337.982 380.208	
<b>CHD<sub>2</sub>OD</b>	$1.06 \times 10^{11} / 9.80 \times 10^{12}$		<sup>2</sup> <sub>02</sub> -1 <sub>01</sub> <sup>3</sup> <sub>03</sub> -2 <sub>02</sub> <sup>4</sup> <sub>04</sub> -3 <sub>03</sub> <sup>5</sup> <sub>05</sub> -4 <sub>04</sub> <sup>6</sup> <sub>06</sub> -5 <sub>05</sub> <sup>7</sup> <sub>07</sub> -6 <sub>06</sub> <sup>8</sup> <sub>08</sub> -7 <sub>07</sub> <sup>9</sup> <sub>09</sub> -8 <sub>08</sub>	78.844 118.264 157.682 197.097 236.509 275.916 315.319 354.716	
<b>CD<sub>3</sub>OD</b>	$1.57 \times 10^7 / 1.13 \times 10^{09}$		<sup>2</sup> <sub>02</sub> -1 <sub>01</sub> <sup>3</sup> <sub>03</sub> -2 <sub>02</sub> <sup>4</sup> <sub>04</sub> -3 <sub>03</sub> <sup>5</sup> <sub>05</sub> -4 <sub>04</sub> <sup>6</sup> <sub>06</sub> -5 <sub>05</sub> <sup>7</sup> <sub>07</sub> -6 <sub>06</sub> <sup>8</sup> <sub>08</sub> -7 <sub>07</sub> <sup>9</sup> <sub>09</sub> -8 <sub>08</sub>	74.035 111.052 148.066 185.078 222.088 259.093 296.095 333.092	
<sup>h</sup> Albertsson et al. (2013) <sup>p2</sup> Parise et al. (2002) <sup>p4</sup> Parise et al. (2004) <sup>p6</sup> Parise et al. (2006) <sup>p9</sup> Parise et al. (2009) <sup>t</sup> Turner et al. (1990) <sup>t</sup> Ceccarelli et al. (1998) <sup>n</sup> Neill et al. (2013) <sup>j</sup> JPL catalog <sup>ni</sup> NIST catalog <sup>c</sup> Coutens et al. (2013) <sup>l</sup> Loinard et al. (2000)					

Table 6: Rotational and distortional constants for different deuterated ions at MP2/6-311G++(d,p) level of theory

Gas phase deuterated species	Rotational constants	Calculated values (in MHz)	Distortional constants	Calculated values (in MHz)
<b>DCO<sup>+</sup></b>	A	-	$D_J$	-
	B	35483.057	$D_{JK}$	-
	C	-	$D_K$	-
			$d_1$	-
			$d_2$	-
<b>N<sub>2</sub>D<sup>+</sup></b>	A	-	$D_J$	-
	B	37491.716	$D_{JK}$	-
	C	-	$D_K$	-
			$d_1$	-
			$d_2$	-
<b>H<sub>2</sub>D<sup>+</sup></b>	A	1309800.71258	$D_J$	$0.1699443269 \times 10^3$
	B	874168.68952	$D_{JK}$	$0.7270365952 \times 10^3$
	C	523857.03868	$D_K$	$0.4076913455 \times 10^3$
			$d_1$	$-0.7957445833 \times 10^2$
			$d_2$	$-0.2957715880 \times 10^2$
<b>H<sub>2</sub>DO<sup>+</sup></b>	A	354117.43200	$D_J$	$0.2947627119 \times 10^1$
	B	216974.71900	$D_{JK}$	$0.2864887879 \times 10^2$
	C	134526.73411	$D_K$	$-0.6322042487 \times 10^0$
			$d_1$	$-0.1844179917 \times 10^1$
			$d_2$	$-0.9521281691 \times 10^0$
<b>HD<sub>2</sub>O<sup>+</sup></b>	A	272194.75777	$D_J$	$0.1776066258 \times 10^1$
	B	177205.99078	$D_{JK}$	$0.1791147098 \times 10^2$
	C	107323.23142	$D_K$	$0.2835585120 \times 10^1$
			$d_1$	$-0.1169643083 \times 10^1$
			$d_2$	$-0.6430195000 \times 10^0$
<b>D<sub>3</sub>O<sup>+</sup></b>	A	177197.36289	$D_J$	$0.7752981475 \times 10^1$
	B	177197.36289	$D_{JK}$	$-0.13674113745 \times 10^2$
	C	88598.68144	$D_K$	$0.6379112348 \times 10^1$
			$d_1$	$0.2872075808 \times 10^{-8}$
			$d_2$	$-0.1219005263 \times 10^{-9}$
<b>HDCN<sup>+</sup></b>	A	183617.60357	$D_J$	$0.5652668773 \times 10^{-1}$
	B	38154.03333	$D_{JK}$	$0.4647653905 \times 10^1$
	C	31588.56408	$D_K$	$0.8915036310 \times 10^1$
			$d_1$	$-0.2020922328 \times 10^{-1}$
			$d_2$	$-0.1513073366 \times 10^{-1}$
<b>D<sub>2</sub>CN<sup>+</sup></b>	A	131072.14036	$D_J$	$0.4973302542 \times 10^{-1}$
	B	35460.00741	$D_{JK}$	$0.3119536865 \times 10^1$
	C	27908.31506	$D_K$	$0.3792274009 \times 10^1$
			$d_1$	$-0.2531909495 \times 10^{-1}$
			$d_2$	$-0.1811095002 \times 10^{-1}$
<b>DCN<sup>+</sup></b>	A	-	$D_J$	-
	B	34105.477	$D_{JK}$	-
	C	-	$D_K$	-
			$d_1$	-
			$d_2$	-
<b>C<sub>3</sub>D<sup>+</sup></b>	A	13126893933.18267	$D_J$	$-0.4042273088 \times 10^6$
	B	-2415470.80371	$D_{JK}$	$0.5378663156 \times 10^7$
	C	818347.68409	$D_K$	$0.2271892620 \times 10^{18}$
			$d_1$	$0.1691184967 \times 10^{-6}$
			$d_2$	$-0.2021136560 \times 10^6$
<b>CD<sup>+</sup></b>	A	-	$D_J$	-
	B	230590.66	$D_{JK}$	-
	C	-	$D_K$	-
			$d_1$	-
			$d_2$	-



Table 7: Calculated and observed rotational transitions of some deuterated ions

Important deuterated ions	Gas Phase Column density (in $\text{cm}^{-2}$ )	Observed/estimated Column density (in $\text{cm}^{-2}$ )	Transitions	Calculated frequency (in GHz)	Comparison (Obs./Theo.)
<b>DCO<sup>+</sup></b>	$1.23 \times 10^{12}$	$4.7 - 40.8 \times 10^{11b}$	1 <sub>01</sub> -0 <sub>00</sub> 2 <sub>02</sub> -1 <sub>01</sub> 3 <sub>03</sub> -2 <sub>02</sub> 4 <sub>04</sub> -3 <sub>03</sub> 5 <sub>05</sub> -4 <sub>04</sub> 6 <sub>06</sub> -5 <sub>05</sub> 7 <sub>07</sub> -6 <sub>06</sub> 8 <sub>08</sub> -7 <sub>07</sub> 9 <sub>09</sub> -8 <sub>08</sub>	70.966 141.932 212.898 283.864 354.830 425.796 496.762 567.728 638.695	72.039 <sup>b</sup> , j, ni 144.077 <sup>b,ni</sup> 216.112 <sup>b,ni</sup> 288.143 <sup>o,ni</sup> 360.169 <sup>ni</sup>
<b>N<sub>2</sub>D<sup>+</sup></b>	$2.40 \times 10^{07}$	$2.310^{12be}$	1 <sub>01</sub> -0 <sub>00</sub> 2 <sub>02</sub> -1 <sub>01</sub> 3 <sub>03</sub> -2 <sub>02</sub> 4 <sub>04</sub> -3 <sub>03</sub> 5 <sub>05</sub> -4 <sub>04</sub> 6 <sub>06</sub> -5 <sub>05</sub> 7 <sub>07</sub> -6 <sub>06</sub> 8 <sub>08</sub> -7 <sub>07</sub> 9 <sub>09</sub> -8 <sub>08</sub>	74.983 149.969 224.952 299.935 374.919 449.902 524.885 599.869 674.852	77.109 <sup>e,ni</sup> 154.217 <sup>e,ni</sup> 231.322 <sup>e,ni</sup>
<b>H<sub>2</sub>D<sup>+</sup></b>	$5.58 \times 10^{12}$	$2 - 40 \times 10^{12c}$			
<b>H<sub>2</sub>DO<sup>+</sup></b>	$1.20 \times 10^{12}$				
<b>HD<sub>2</sub>O<sup>+</sup></b>	$2.41 \times 10^{12}$				
<b>D<sub>3</sub>O<sup>+</sup></b>	$1.92 \times 10^{09j}$				
<b>HDCN<sup>+</sup></b>	$2.55 \times 10^{12}$		1 <sub>01</sub> -0 <sub>00</sub> 2 <sub>02</sub> -1 <sub>01</sub> 3 <sub>03</sub> -2 <sub>02</sub> 4 <sub>04</sub> -3 <sub>03</sub> 5 <sub>05</sub> -4 <sub>04</sub> 6 <sub>06</sub> -5 <sub>05</sub> 7 <sub>07</sub> -6 <sub>06</sub> 8 <sub>08</sub> -7 <sub>07</sub> 9 <sub>09</sub> -8 <sub>08</sub>	69.746 139.486 209.222 278.951 348.673 418.384 488.082 557.766 627.433	
<b>D<sub>2</sub>CN<sup>+</sup></b>	$1.96 \times 10^{08}$		2 <sub>02</sub> -1 <sub>01</sub> 3 <sub>03</sub> -2 <sub>02</sub> 4 <sub>04</sub> -3 <sub>03</sub> 5 <sub>05</sub> -4 <sub>04</sub> 6 <sub>06</sub> -5 <sub>05</sub> 7 <sub>07</sub> -6 <sub>06</sub> 8 <sub>08</sub> -7 <sub>07</sub> 9 <sub>09</sub> -8 <sub>08</sub>	126.738 190.099 253.455 316.802 380.139 443.463 506.773 570.067	
<b>DCN<sup>+</sup></b>	$8.93 \times 10^{11}$		2 <sub>02</sub> -1 <sub>01</sub> 3 <sub>03</sub> -2 <sub>02</sub> 4 <sub>04</sub> -3 <sub>03</sub> 5 <sub>05</sub> -4 <sub>04</sub> 6 <sub>06</sub> -5 <sub>05</sub> 7 <sub>07</sub> -6 <sub>06</sub> 8 <sub>08</sub> -7 <sub>07</sub> 9 <sub>09</sub> -8 <sub>08</sub>	136.433 204.641 272.851 341.062 409.273 477.484 545.695 613.906	
<b>C<sub>3</sub>D<sup>+</sup></b>	$2.37 \times 10^{10}$		4 <sub>04</sub> -3 <sub>03</sub> 5 <sub>05</sub> -4 <sub>04</sub> 6 <sub>06</sub> -5 <sub>05</sub> 7 <sub>07</sub> -6 <sub>06</sub> 8 <sub>08</sub> -7 <sub>07</sub> 9 <sub>09</sub> -8 <sub>08</sub>	79.144 98.930 118.716 138.502 158.289 178.075	
<b>CD<sup>+</sup></b>	$6.02 \times 10^{11}$		1 <sub>01</sub> -0 <sub>00</sub> 2 <sub>02</sub> -1 <sub>01</sub>	461.181 922.362	
<sup>e</sup> Emprechtinger et al. (2008) <sup>o</sup> Miettinen et al. (2012) <sup>b</sup> Butner et al. (1995) <sup>b</sup> Bergman et al. (2010) <sup>c</sup> Caselli et al. (2008) <sup>j</sup> JPL catalog <sup>j</sup> NIST catalog					

Table 8: Vibrational frequencies of different isotopomers in gas/ice phase at B3LYP/6-311++G level of theory

Deuterated species in ice Phase	Isotopomers	Peak positions (in $\text{cm}^{-1}$ ) (Gas phase)	Absorbance	Peak positions (in $\text{cm}^{-1}$ ) ( $\text{H}_2\text{O}$ ice)	Absorbance	Experimental peak positions (in gas phase) (in $\text{cm}^{-1}$ )
$\text{H}_2\text{O}$	$\text{HDO}$	1378.16 2705.63 3735.97	88.6531 7.2636 19.1116	1405.66 2702.10 3727.40	122.7328 15.7450 41.5054	
	$\text{D}_2\text{O}$	1154.12 2619.48 2800.44	54.8490 0.8079 19.4060	1176.99 2625.06 2785.31	76.6104 0.9352 43.7223	
$\text{H}_2\text{CO}$	$\text{HDCO}$	1045.23 1100.30 1439.70 1677.21 2186.27 2975.90	6.7359 5.5420 8.2712 81.6357 64.9183 89.0502	1040.78 1108.30 1431.17 1649.89 2213.81 3014.48	11.6072 7.3579 20.5150 136.6138 68.0555 80.8224	
	$\text{D}_2\text{CO}$	972.36 999.70 1138.09 1650.97 2132.09 2248.26	1.8692 7.7724 1.9191 75.4535 56.4735 82.5199	978.72 995.53 1131.49 1623.04 2154.89 2281.63	2.2770 13.1905 5.5560 134.8462 68.6649 75.1423	
$\text{CH}_3\text{OH}$	$\text{CD}_3\text{OD}$	161.20 293.34 386.80 500.29 763.50 895.12 1048.29 1174.20 2082.62 2214.55 2576.92 2838.59	99.5390 110.3155 35.4860 58.7503 2.4498 1.2200 9.7550 47.4951 69.9112 50.2665 22.3665 94.7827	220.66 764.12 884.65 924.45 1037.46 1097.12 1103.99 1126.51 2158.35 2286.64 2326.38 2678.17	142.0151 45.5776 3.6340 75.5395 17.1796 4.6425 5.7715 9.9785 39.6044 41.3044 23.5277 18.9233	773.2 <sup>m</sup> 895 <sup>m</sup> 1031.5 <sup>m</sup> 1032.56 <sup>m</sup> 2077.8 <sup>m</sup> 2218.1 <sup>m</sup>
		164.48 332.46 392.77 515.29 1045.77 1153.64 1176.82 1428.83 2576.98 2837.68 2883.82 2984.23	100.7205 132.7390 34.8017 63.2073 7.7157 8.1762 54.5779 12.8712 22.7108 126.7372 116.3223 109.4862	231.34 819.72 925.19 989.82 1173.40 1342.95 1385.44 1506.41 2236.69 2677.74 3047.59 3134.09	134.7124 43.8757 85.1056 21.8331 0.8951 7.8599 3.5271 10.0101 40.6041 20.6087 63.7930 36.2857	1048.5 <sup>m1</sup> 1162.5 <sup>m1</sup> 1162.5 <sup>m1</sup> 1460.5 <sup>m1</sup> 2884±4 <sup>m1</sup> 2990±4 <sup>m1</sup>
		162.53 307.05 389.58 508.25 820.84 1095.81 1174.20 1270.89 2135.97 2577.06 2838.39 2951.19	99.7778 116.6308 36.0346 58.9529 2.4061 16.1715 46.4322 13.1683 69.7468 22.0773 101.4147 110.0932	225.69 800.46 886.01 932.91 1098.79 1110.48 1353.75 1369.50 2190.28 2286.72 2677.74 3125.89	139.9513 41.1593 3.8315 101.7461 0.1321 10.2463 10.4653 2.3322 39.8542 41.6627 20.7812 33.0746	814.8 <sup>m1</sup> 1096.4 <sup>m1</sup> 2133 <sup>m</sup> 2930 <sup>m</sup>
		165.64 372.84 393.54 583.35 829.61 1100.93 1270.48 1408.11 2135.99 2614.16 2951.01 3850.10	92.4334 169.9004 70.3956 82.7371 2.7927 21.6663 16.4612 71.7012 70.2213 44.8765 117.0050 131.9254	292.47 886.08 914.18 945.61 1110.45 1270.82 1353.75 1393.25 2190.34 2286.72 3125.42 3677.98	266.3570 3.2353 0.3106 150.2974 10.4543 24.1712 10.5085 12.8091 40.6166 41.4842 35.0867 25.2741	1096.6 <sup>m1</sup> 1269 <sup>m1</sup> 2133.5 <sup>m</sup> 2944.5 <sup>m</sup>

Deuterated species in ice Phase	Isotopomers	Peak positions (in $\text{cm}^{-1}$ ) (Gas phase)	Absorbance	Peak positions (in $\text{cm}^{-1}$ ) ( $\text{H}_2\text{O}$ ice)	Absorbance	Experimental peak positions (in $\text{cm}^{-1}$ )
<b><math>\text{CH}_3\text{OH}</math></b>	<b><math>\text{CH}_2\text{DOH}</math></b>	169.30 384.91 404.02 596.94 1046.19 1162.78 1401.57 1435.51 2613.89 2883.09 2984.23 3850.11	92.7351 106.3536 146.5793 93.4742 6.7389 21.4716 68.1558 17.0692 48.0499 145.3978 110.7735 131.7588	296.56 905.41 951.71 1058.02 1284.07 1368.15 1390.61 1506.54 2236.72 3047.58 3133.63 3678.00	259.9902 2.0358 149.3625 9.8248 25.1187 8.5425 10.2958 10.0133 40.9083 63.8841 37.9938 25.3322	1050 $\pm$ 2 <sup>m1</sup>       1460 $\pm$ 1 <sup>m1</sup>  2886 $\pm$ 1 <sup>m1</sup> 2980 $\pm$ 5 <sup>m1</sup>
	<b><math>\text{CH}_3\text{OD}</math></b>	199.80 338.75 412.80 567.48 1046.35 1155.43 1410.22 1437.98 2787.74 2882.55 2984.23 3613.98	213.36 100.46 18.84 99.9472 5.8887 15.0893 26.2351 53.5992 54.5346 149.1114 109.6645 131.49	239.23 851.97 955.71 1153.40 1231.89 1485.36 1514.64 1522.56 2677.74 3013.36 3082.00 3138.31	126.49 70.54 78.61 0.4680 0.2061 2.5672 11.1257 12.4155 20.3561 61.4815 68.9276 36.6364	1042.8 <sup>m</sup> 1142 $\pm$ 3 <sup>m1</sup>   1421.3 <sup>m1</sup>  2896.5 <sup>m1</sup> 2970 $\pm$ 4 <sup>m1</sup>
<b><math>\text{HCN}</math></b>	<b><math>\text{DCN}</math></b>	616.73 1943.99 2714.94	28.3201 6.7499 26.1260	628.94 1939.11 2702.60	28.1769 25.4985 35.1536	
<b><math>\text{HNC}</math></b>	<b><math>\text{DNC}</math></b>	477.88 1942.58 2886.22	113.6888 34.7245 181.4461	478.34 1955.07 2855.45	131.2467 29.1366 292.3229	
<sup>m</sup> Serrallach, Meyer & Gunthard 1974(Ar matrix data) <sup>m1</sup> Serrallach, Meyer & Gunthard 1974(vapour)						

Table 9: Vibrational frequencies of different deuterated ions in gas phase at B3LYP/6-311++G level of theory

Gas phase deuterated ions deuterated ions	Peak positions (gas phase) (Wavenumber) (in $\text{cm}^{-1}$ )	Absorbance
<b>DCO<sup>+</sup></b>	683.57 1897.22 2624.76	3.3998 132.8371 25.3446
<b>N<sub>2</sub>D<sup>+</sup></b>	628.33 2047.85 2730.37	87.6580 49.4619 290.2813
<b>H<sub>2</sub>D<sup>+</sup></b>	2230.79 2345.31 3015.87	66.6525 317.0829 76.1241
<b>HD<sub>2</sub><sup>+</sup></b>	1946.29 2098.01 2733.51	158.8752 87.1753 126.7451
<b>H<sub>2</sub>DO<sup>+</sup></b>	566.82 1415.30 1695.32 2675.50 3639.63 3742.37	856.4178 118.6293 188.8344 145.2111 201.6169 504.7184
<b>HD<sub>2</sub>O<sup>+</sup></b>	518.63 1246.29 1557.51 2599.43 2760.07 3694.16	685.2860 79.5791 149.7999 59.0382 265.0375 364.9741
<b>HDCN<sup>+</sup></b>	313.84 838.27 970.70 1781.07 2139.99 2867.97	3.8689 94.7313 131.1481 12.5791 211.2602 378.5943
<b>D<sub>2</sub>CN<sup>+</sup></b>	288.00 742.61 802.03 1737.90 2116.60 2157.11	1.1228 51.1535 76.3573 0.3969 159.4864 265.8839
<b>D<sub>3</sub>O<sup>+</sup></b>	465.38 1241.35 1241.36 2529.44 2759.90 2759.90	515.2134 77.8866 77.8855 0.0000 260.9641 260.9620
<b>CD<sup>+</sup></b>	2011.51	0.9199
<b>C<sub>3</sub>D<sup>+</sup></b>	248.79 705.87 711.54 1158.20 2022.23 2605.23	4.8847 2.3408 3.0668 54.3460 834.8943 46.2760
<b>DCN<sup>+</sup></b>	617.26 1943.59 2714.08	28.3187 6.7620 26.1128